Nonlinear Dyn (2008) 52: 159–179
DOI 10.1007/s11071-007-9269-3

ORIGINAL PAPER

Deployment/retrieval optimization for flexible tethered satellite systems

Paul Williams

Received: 6 November 2006 / Accepted: 2 April 2007 / Published online: 7 June 2007
© Springer Science+Business Media, Inc. 2007

Abstract A methodology for deployment/retrieval optimization of tethered satellite systems is presented. Previous research has focused on the case where the tether is modeled as an inelastic, straight rod for the determination of optimal system trajectories. However, the tether shape and string vibrations can often be very important, particularly when the deployment/retrieval speed changes rapidly, or when external forces such as aerodynamic drag or electrodynamic forces are present. An efficient mathematical model for flexible tethered systems is first derived, which treats the tether as composed of a system of lumped masses connected via inelastic links. A tension control law is presented based on a discretization of the tether length dynamics via Chebyshev polynomials. A scheme that minimizes the second derivative of length over the trajectory based on physically meaningful coefficients is presented. This is utilized in conjunction with evolutionary optimization methods to minimize the rigid body and flexible modes of the system during deployment/retrieval. It is shown that only a very small number of parameters are required to generate accurate trajectories. The results are compared to the case where the tether is modeled as a straight rod.

P. Williams (✉)
1/4 Maylands Ave, Balwyn North, VIC 3104, Australia
e-mail: tethered.systems@gmail.com

Keywords Tethered satellites · Deployment/retrieval · Optimal control · Flexible systems · Evolutionary control

1 Introduction

The deployment/retrieval of satellites via tethers in space is a problem that has been studied rather extensively [1–5]. However, accurate closed-loop control has only been demonstrated in practice via the Small Expendable Deployer System II (SEDS-II), which deployed a 20-km-long tether and subsatellite to the local vertical [6]. The success of both SEDS-I (which utilized an open-loop control scheme) and SEDS-II was due in large part to the deployment hardware, which was considerably simpler than that used by the Tethered Subsatellite System 1 (TSS-1), which jammed early during the deployment phase. The major difference in the deployment hardware lies in the fact that the SEDS deployer uses a passive, friction-brake to control the speed of the deployment whereas the TSS-1 mission used an active deployer driven by a reel mechanism [7].

Over the years, many control schemes have been developed for deploying/retrieving tethered satellite systems [8–16]. This has been aided by the fact that deployment is inherently stable provided certain deployment speeds are not exceeded. The retrieval process on the other hand is known to be unstable.

This is true of both the lateral and librational (rigid body) modes. Combinations of open-loop and closed-loop control schemes have been proposed, although few are generally applicable to many missions due to tight physical constraints imposed by the ejection parameters of the subsatellite and other practical limitations. To deal with the many constraints imposed by real hardware, it is necessary to solve a two-point boundary value problem that arises by applying optimal control theory to the deployment problem. Optimal control is the only framework that is currently capable of dealing with the complex nonlinear control problem.

The application of optimal control methodology to tether deployment/retrieval was first presented by Fujii and Anazawa [2], who minimized a combination of the square of the tether tension and the in-plane libration angle. In their work, the tether was treated as massless and any external perturbations were neglected. Zimmerman et al. [16] determined trajectories for a tether-assisted re-entry mission so as to minimize the square of the tether tension assuming a massless tether. However, the effects of tether flexibility were neglected. Koakutsu et al. [15] considered optimal deployment control for a microsatellite to minimize the integral square of the tether length rate, and also included a term in the cost function to keep the tether tension large. This particular cost function was selected based on the ability of a tracking controller to follow the trajectory in the presence of disturbances. The optimal trajectory was simulated in a multibody flexible tether model, thus accounting for the additional disturbances not inherent in the control model. The tracking controller was based on a Lyapunov tracking scheme originally considered by Fujii and Anazawa [2]. Williams et al. [17] considered the design of optimal trajectories for the Young Engineers Satellite 2 (YES2) mission accounting for tether mass, orbit eccentricity, and aerodynamic drag on the tether. The trajectories were designed taking into account a variety of important constraints for the deployment hardware. The trajectories were simulated in a flexible tether model with disturbances and a feedback controller. The effects of tether flexibility can result in some differences in the trajectories, particularly for large disturbances from the nominal.

This paper is motivated by the YES2 mission, which proposes to deploy a small payload via a tether to enable the payload to re-enter the Earth's atmosphere and land safely. This is achieved by using inherent dynamical properties of a deploying tether, which induces a swinging motion that opposes the orbital velocity on the first swing through the local vertical. For a sufficiently long tether, the swing amplitude does not have to be particularly large to achieve the necessary delta-v to deorbit the payload.

Deployment optimizations are often carried out under the assumption of an inflexible tether. The tether librations are the fundamental mode of the system that must be considered in the control design. Usually, the libration dynamics are considered to be very important because of the absence of sufficient damping in space. Structural damping is able to help mitigate longitudinal oscillations, but is relatively ineffective for damping other modes of vibration. The libration dynamics, as observed using simplified models, tend to propagate more or less faithfully into more complex models in many studies. The caveat is that this is not always the case with control systems designed via tension control. Under certain circumstances, such as low tension, rapidly changing tension, or significant external disturbances, the tether dynamics can differ considerably. Examples of disturbances are aerodynamic drag and electrodynamic forces. In the case of YES2, the orbital altitude is low enough that drag is a significant force acting on the tether. In order to validate a particular control law and continue with further analysis, it is necessary to employ more sophisticated models that account for the lateral modes of the tether. Furthermore, it is also desirable to have a general methodology for optimizing the trajectories of flexible tethers rather than inflexible tethers. It is the purpose of this paper to develop an effective methodology for the optimization of tether deployment/retrieval trajectories for the general case of a flexible tethered system.

2 Mathematical modeling of tethered satellite systems for control design

The predominant modeling assumption that is used in the literature insofar as control of tethered satellite systems is concerned is that the system can be modeled with three degrees of freedom [2–5]. In other words, when dealing with the librational motion of the system, it is sufficient to model it using spherical coordinates representing the dynamics of the subsatellite. This effectively treats the tether as a straight body, which can either be modeled as an inelastic or elastic rod. Early work has neglected the tether mass since

its contribution to the librational motion can be considered relatively small [2]. This is due to the fact that the tether is axisymmetric. When large changes in length are considered, the effect of tether mass becomes more important. Moreover, it is essential to include the effects of tether mass when designing tension control laws because there is a nonlinear relationship between tension and tether mass. However, when performing preliminary analyses, it is sufficient to ignore such effects and compensate for these later in the design.

Although the assumption of treating the tether as a straight rod is often a good one, it can create some problems in practice. For example, all tether string vibrations are neglected, which play a very important role in electrodynamic systems or systems subjected to long-term perturbations. Furthermore, large changes in deployment velocity can induce significant distortions to the tether shape, which ultimately affects the accuracy of the deployment control laws. Earlier work focused much attention on the dynamics of tethers during length changes, particularly retrieval [1]. In the earlier work, assumed modes was typically the method of choice [10]. However, where optimal control methods are employed, high frequency dynamics can be difficult to handle even with modern methods. For this reason, most optimal deployment/retrieval schemes consider the tether as inelastic. The following subsection presents a rather general model for the dynamics of a tethered satellite system in orbit around a spherical planet. This model is simplified for later use in deployment/retrieval optimization.

2.1 Straight, inelastic tether model

In this model, the tether is assumed to be straight and inextensible, uniform in mass, the end masses are assumed to be point masses, and the tether is deployed from one end mass only. A representation of the model, as well as the generalized coordinates used to describe the motion, is shown in Fig. 1. The generalized coordinates are selected as the orbit radius to the center of mass, R, right ascension of the center of mass, α, the declination of the center of mass, δ, the tether in-plane libration angle, θ, the out-of-plane tether libration angle, ϕ, and the tether length, l.

The radius vector to the center of mass may be written in inertial coordinates as

$$\mathbf{R} = R\cos\delta\cos\alpha\mathbf{i} + R\cos\delta\sin\alpha\mathbf{j} + R\sin\delta\mathbf{k} \tag{1}$$

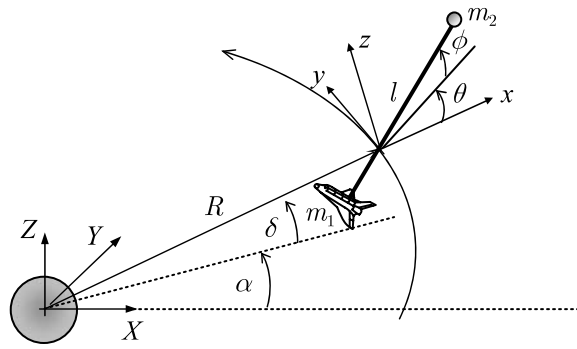

Fig. 1 General simplified tether dynamical model

from which the kinetic energy due to translation of the center of mass is derived as

$$T_{\mathrm{t}} = \frac{1}{2}m\left(\dot{R}^2 + R^2\dot{\delta}^2 + R^2\dot{\alpha}^2\cos^2\delta\right) \tag{2}$$

where $m = m_1 + m_t + m_2$ is the total system mass, $m_1 = m_1^0 - m_t$ is the mass of the mother satellite, m_t is the tether mass, m_2 is the subsatellite mass, and m_1^0 is the mass of the mother satellite prior to deployment of the tether.

The rotational kinetic energy is determined via

$$T_{\mathrm{r}} = \frac{1}{2}\boldsymbol{\omega}^T[I]\boldsymbol{\omega} \tag{3}$$

where $\boldsymbol{\omega}$ is the inertial angular velocity of the tether in the tether body frame

$$\begin{aligned}\boldsymbol{\omega} = {} & (\dot{\alpha}\sin\delta\cos\theta\cos\phi - \dot{\delta}\sin\theta\cos\phi \\ & + \dot{\alpha}\cos\delta\sin\phi + \dot{\theta}\sin\phi)\mathbf{i} \\ & + (-\dot{\phi} - \dot{\alpha}\sin\delta\sin\theta - \dot{\delta}\cos\theta)\mathbf{j} \\ & + (-\dot{\alpha}\sin\delta\cos\theta\sin\phi + \dot{\delta}\sin\theta\sin\phi \\ & + \dot{\alpha}\cos\delta\cos\phi + \dot{\theta}\cos\phi)\mathbf{k}.\end{aligned} \tag{4}$$

Thus we have that

$$\begin{aligned}T_{\mathrm{r}} = {} & \frac{1}{2}m^*l^2\big[(\dot{\phi} + \dot{\alpha}\sin\delta\sin\theta + \dot{\delta}\cos\theta)^2 \\ & + (\dot{\delta}\sin\theta\sin\phi - \dot{\alpha}\sin\delta\cos\theta\sin\phi \\ & + \dot{\alpha}\cos\delta\cos\phi + \dot{\theta}\cos\phi)^2\big]\end{aligned} \tag{5}$$

and $m^* = (m_1 + \frac{m_t}{2})(m_2 + \frac{m_t}{2})/m - m_t/6$ is the system reduced mass. The kinetic energy due to deployment is obtained as

$$T_{\mathrm{e}} = \frac{1}{2}\frac{m_1(m_2 + m_t)}{m}\dot{l}^2 \tag{6}$$

which accounts for the fact that the tether is modeled as stationary inside the deployer and is accelerated to the deployment velocity after exiting the deployer. This introduces a thrust-like term into the equations of motion, which affects the value of the tether tension [17].

The system gravitational potential energy is (assuming a second order gravity-gradient expansion)

$$V = -\frac{\mu m}{R} + \frac{\mu m^* l^2}{2R^3}\left(1 - 3\cos^2\theta\cos^2\phi\right). \tag{7}$$

The Lagrangian may be formed as

$$\begin{aligned} L = {} & \frac{1}{2}m\left(\dot{R}^2 + R^2\dot{\delta}^2 + R^2\dot{\alpha}^2\cos^2\delta\right) \\ & + \frac{1}{2}m^* l^2\big[(\dot{\phi} + \dot{\alpha}\sin\delta\sin\theta + \dot{\delta}\cos\theta)^2 \\ & + (\dot{\delta}\sin\theta\sin\phi - \dot{\alpha}\sin\delta\cos\theta\sin\phi \\ & + \dot{\alpha}\cos\delta\cos\phi + \dot{\theta}\cos\phi)^2\big] \\ & + \frac{1}{2}\frac{m_1(m_2+m_t)}{m}\dot{l}^2 + \frac{\mu m}{R} \\ & - \frac{\mu m^* l^2}{2R^3}\left(1 - 3\cos^2\theta\cos^2\phi\right). \end{aligned} \tag{8}$$

By utilizing Lagrange's equations, the equations of motion for the system are obtained as

$$\begin{aligned} & m\ddot{R} - mR\dot{\delta}^2 - mR\dot{\alpha}^2\cos^2\delta + \frac{\mu m}{R^2} \\ & - \frac{3\mu m^* l^2}{2R^4}\left(1 - 3\cos^2\theta\cos^2\phi\right) = Q_R, \end{aligned} \tag{9}$$

$$\begin{aligned} & 2mR\dot{R}\dot{\alpha}\cos^2\delta + mR^2\ddot{\alpha}\cos^2\delta - 2mR^2\dot{\alpha}\dot{\delta}\sin\delta\cos\delta \\ & + \dot{m}^* l^2\big[\gamma_1\sin\delta\sin\theta + \gamma_2(\cos\delta\cos\phi \\ & - \sin\delta\cos\theta\sin\phi)\big] + 2m^* l\dot{l}\big[\gamma_1\sin\delta\sin\theta \\ & + \gamma_2(\cos\delta\cos\phi - \sin\delta\cos\theta\sin\phi)\big] \\ & + m^* l^2\big[(\ddot{\phi} + \ddot{\alpha}\sin\delta\sin\theta + \dot{\alpha}\dot{\delta}\cos\delta\sin\theta \\ & + \dot{\alpha}\dot{\theta}\sin\delta\cos\theta + \ddot{\delta}\cos\theta - \dot{\delta}\dot{\theta}\sin\theta)\sin\delta\sin\theta \\ & + \gamma_1(\dot{\delta}\cos\delta\sin\theta + \dot{\theta}\sin\delta\cos\theta) + (\ddot{\delta}\sin\theta\sin\phi \\ & + \dot{\delta}\dot{\theta}\cos\theta\sin\phi + \dot{\delta}\dot{\phi}\sin\theta\cos\phi \\ & - \ddot{\alpha}\sin\delta\cos\theta\sin\phi - \dot{\alpha}\dot{\delta}\cos\delta\cos\theta\sin\phi \\ & + \dot{\alpha}\dot{\theta}\sin\delta\sin\theta\sin\phi - \dot{\alpha}\dot{\phi}\sin\delta\cos\theta\cos\phi \\ & + \ddot{\alpha}\cos\delta\cos\phi - \dot{\alpha}\dot{\delta}\sin\delta\cos\phi \\ & - \dot{\alpha}\dot{\phi}\cos\delta\sin\phi + \ddot{\theta}\cos\phi \\ & - \dot{\theta}\dot{\phi}\sin\phi)(\cos\delta\cos\phi - \sin\delta\cos\theta\sin\phi) \\ & + \gamma_2(\dot{\theta}\sin\delta\sin\theta\sin\phi - \dot{\delta}\sin\delta\cos\phi \\ & - \dot{\phi}\cos\delta\sin\phi - \dot{\delta}\cos\delta\cos\theta\sin\phi \\ & - \dot{\phi}\sin\delta\cos\theta\cos\phi)\big] = Q_\alpha, \end{aligned} \tag{10}$$

$$\begin{aligned} & 2mR\dot{R}\dot{\delta} + mR^2\ddot{\delta} + \dot{m}^* l^2[\gamma_1\cos\theta + \gamma_2\sin\theta\sin\phi] \\ & + 2m^* l\dot{l}[\gamma_1\cos\theta + \gamma_2\sin\theta\sin\phi] \\ & + m^* l^2\big[(\ddot{\phi} + \ddot{\alpha}\sin\delta\sin\theta + \dot{\alpha}\dot{\delta}\cos\delta\sin\theta \\ & + \dot{\alpha}\dot{\theta}\sin\delta\cos\theta + \ddot{\delta}\cos\theta - \dot{\delta}\dot{\theta}\sin\theta)\cos\theta \\ & - \gamma_1\dot{\theta}\sin\theta + (\ddot{\delta}\sin\theta\sin\phi + \dot{\delta}\dot{\theta}\cos\theta\sin\phi \\ & + \dot{\delta}\dot{\phi}\sin\theta\cos\phi - \ddot{\alpha}\sin\delta\cos\theta\sin\phi \\ & - \dot{\alpha}\dot{\delta}\cos\delta\cos\theta\sin\phi + \dot{\alpha}\dot{\theta}\sin\delta\sin\theta\sin\phi \\ & - \dot{\alpha}\dot{\phi}\sin\delta\cos\theta\cos\phi + \ddot{\alpha}\cos\delta\cos\phi \\ & - \dot{\alpha}\dot{\delta}\sin\delta\cos\phi - \dot{\alpha}\dot{\phi}\cos\delta\sin\phi + \ddot{\theta}\cos\phi \\ & - \dot{\theta}\dot{\phi}\sin\phi)\sin\theta\sin\phi + \gamma_2(\dot{\theta}\cos\theta\sin\phi \\ & + \dot{\phi}\sin\theta\cos\phi)\big] + mR^2\dot{\alpha}^2\sin\delta\cos\delta \\ & - m^* l^2\big[\gamma_1\dot{\alpha}\cos\delta\sin\theta - \gamma_2(\dot{\alpha}\cos\delta\cos\theta\sin\phi \\ & + \dot{\alpha}\sin\delta\cos\phi)\big] = Q_\delta, \end{aligned} \tag{11}$$

$$\begin{aligned} & \dot{m}^* l^2\gamma_2\cos\phi + 2m^* l\dot{l}\gamma_2\cos\phi + m^* l^2\big[(\ddot{\delta}\sin\theta\sin\phi \\ & + \dot{\delta}\dot{\theta}\cos\theta\sin\phi + \dot{\delta}\dot{\phi}\sin\theta\cos\phi \\ & - \ddot{\alpha}\sin\delta\cos\theta\sin\phi - \dot{\alpha}\dot{\delta}\cos\delta\cos\theta\sin\phi \\ & + \dot{\alpha}\dot{\theta}\sin\delta\sin\theta\sin\phi - \dot{\alpha}\dot{\phi}\sin\delta\cos\theta\cos\phi \\ & + \ddot{\alpha}\cos\delta\cos\phi - \dot{\alpha}\dot{\delta}\sin\delta\cos\phi \\ & - \dot{\alpha}\dot{\phi}\cos\delta\sin\phi + \ddot{\theta}\cos\phi - \dot{\theta}\dot{\phi}\sin\phi)\cos\phi \\ & - \gamma_2\dot{\phi}\sin\phi\big] - m^* l^2\big[\gamma_1(\dot{\alpha}\sin\delta\cos\theta - \dot{\delta}\sin\theta) \\ & + \gamma_2(\dot{\delta}\cos\theta\sin\phi + \dot{\alpha}\sin\delta\sin\theta\sin\phi)\big] \\ & + \frac{3\mu m^* l^2}{R^3}\sin\theta\cos\theta\cos^2\phi = Q_\theta, \end{aligned} \tag{12}$$

$$\begin{aligned} & \dot{m}^* l^2\gamma_1 + 2m^* l\dot{l}\gamma_1 \\ & + m^* l^2(\ddot{\phi} + \ddot{\alpha}\sin\delta\sin\theta + \dot{\alpha}\dot{\delta}\cos\delta\sin\theta \\ & + \dot{\alpha}\dot{\theta}\sin\delta\cos\theta + \ddot{\delta}\cos\theta - \dot{\delta}\dot{\theta}\sin\theta) \\ & - m^* l^2\big[\gamma_2(\dot{\delta}\sin\theta\cos\phi - \dot{\alpha}\sin\delta\cos\theta\cos\phi \end{aligned}$$

$$- \dot{\alpha}\cos\delta\sin\phi - \dot{\theta}\sin\phi)\big] + \frac{3\mu m^* l^2}{R^3}\sin\phi\cos\phi\cos^2\theta = Q_\phi, \tag{13}$$

$$\dot{m}^{\#}\dot{l} + m^{\#}\ddot{l} - \frac{1}{2}\big(m^*\big)' l^2\big[\gamma_1^2 + \gamma_2^2\big] - m^* l\big[\gamma_1^2 + \gamma_2^2\big] - \frac{1}{2}\big(m^{\#}\big)'\dot{l}^2 + \frac{\mu(m^*)' l^2}{2R^3}\big(1 - 3\cos^2\theta\cos^2\phi\big) + \frac{\mu m^* l}{R^3}\big(1 - 3\cos^2\theta\cos^2\phi\big) = -T \tag{14}$$

where

$$\gamma_1 = \dot{\phi} + \dot{\alpha}\sin\delta\sin\theta + \dot{\delta}\cos\theta, \tag{15}$$

$$\gamma_2 = \dot{\delta}\sin\theta\sin\phi - \dot{\alpha}\sin\delta\cos\theta\sin\phi + \dot{\alpha}\cos\delta\cos\phi + \dot{\theta}\cos\phi, \tag{16}$$

$$\gamma_3 = \dot{\delta}\dot{\theta}\cos\theta\sin\phi + \dot{\delta}\dot{\phi}\sin\theta\cos\phi - \dot{\alpha}\dot{\delta}\cos\delta\cos\theta\sin\phi + \dot{\alpha}\dot{\theta}\sin\delta\sin\theta\sin\phi - \dot{\alpha}\dot{\phi}\sin\delta\cos\theta\cos\phi - \dot{\alpha}\dot{\delta}\sin\delta\cos\phi - \dot{\alpha}\dot{\phi}\cos\delta\sin\phi - \dot{\theta}\dot{\phi}\sin\phi, \tag{17}$$

$$\dot{m}^* = \frac{\rho\dot{l}}{2}\frac{(m_1 - m_2)}{m} - \frac{\rho\dot{l}}{6}, \tag{18}$$

$$\dot{m}^{\#} = \rho\dot{l}\frac{(2m_1 - m)}{m}, \tag{19}$$

$$\big(m^*\big)' = \frac{\rho}{2}\frac{(m_1 - m_2)}{m} - \frac{\rho}{6}, \tag{20}$$

$$\big(m^{\#}\big)' = \rho\frac{(2m_1 - m)}{m}. \tag{21}$$

In the simplified case, it is sufficient to treat the dynamics of the tether system as being confined to a constant orbital plane. Thus, by substitution of $\delta = 0$ into the above equations, the following simplified equations of motion are obtained

$$m\ddot{R} - mR\dot{\alpha}^2 + \frac{\mu m}{R^2} - \frac{3\mu m^* l^2}{2R^4}\big(1 - 3\cos^2\theta\cos^2\phi\big) = Q_R, \tag{22}$$

$$2mR\dot{R}\dot{\alpha} + mR^2\ddot{\alpha} + \dot{m}^* l^2\big[(\dot{\alpha} + \dot{\theta})\cos^2\phi\big] + 2m^* l\dot{l}\big[(\dot{\alpha} + \dot{\theta})\cos^2\phi\big] + m^* l^2\big[(\ddot{\alpha} + \ddot{\theta})\cos^2\phi - 2(\dot{\alpha} + \dot{\theta})\dot{\phi}\cos\phi\sin\phi\big] = Q_\alpha, \tag{23}$$

$$\dot{m}^* l^2(\dot{\alpha} + \dot{\theta})\cos^2\phi + 2m^* l\dot{l}(\dot{\alpha} + \dot{\theta})\cos^2\phi + m^* l^2\big[(\ddot{\alpha} + \ddot{\theta})\cos^2\phi - 2(\dot{\alpha} + \dot{\theta})\dot{\phi}\cos\phi\sin\phi\big] + \frac{3\mu m^* l^2}{R^3}\sin\theta\cos\theta\cos^2\phi = Q_\theta, \tag{24}$$

$$\dot{m}^* l^2\dot{\phi} + 2m^* l\dot{l}\dot{\phi} + m^* l^2\ddot{\phi} + m^* l^2(\dot{\alpha} + \dot{\theta})^2\sin\phi\cos\phi + \frac{3\mu m^* l^2}{R^3}\sin\phi\cos\phi\cos^2\theta = Q_\phi, \tag{25}$$

$$\dot{m}^{\#}\dot{l} + m^{\#}\ddot{l} - \frac{1}{2}\big(m^*\big)' l^2\big[\dot{\phi}^2 + (\dot{\alpha} + \dot{\theta})^2\cos^2\phi\big] - m^* l\big[\dot{\phi}^2 + (\dot{\alpha} + \dot{\theta})^2\cos^2\phi\big] - \frac{1}{2}\big(m^{\#}\big)'\dot{l}^2 + \frac{\mu(m^*)' l^2}{2R^3}\big(1 - 3\cos^2\theta\cos^2\phi\big) + \frac{\mu m^* l}{R^3}\big(1 - 3\cos^2\theta\cos^2\phi\big) = -T \tag{26}$$

where it must be recognized that α now represents the orbit true anomaly.

2.1.1 Simplifications for deployment/retrieval optimization

When deployment and retrieval of the system is considered, the time spans involved are typically small compared to total mission times. Therefore, a good approximation is to assume that the orbit remains unperturbed. The validity of this assumption depends on the mass of the mother satellite compared to the subsatellite and tether mass. If this ratio is large, then the approximation is a good one. Under the assumption of a Keplerian reference orbit for the center of mass, the nondimensional equations of motion can be written as

$$\theta'' = 2(\theta' + 1)\left[\frac{e\sin\nu}{\kappa} + \phi'\tan\phi - \frac{m_1(m_2 + \frac{m_t}{2})}{mm^*}\frac{\Lambda'}{\Lambda}\right] - \frac{3}{\kappa}\sin\theta\cos\theta + \frac{Q_\theta}{m^*\Lambda^2 L_r^2\dot{\nu}^2\cos^2\phi}, \tag{27}$$

$$\phi'' = \frac{2e\sin\nu}{\kappa}\phi' - 2\frac{m_1(m_2 + \frac{m_t}{2})}{mm^*}\frac{\Lambda'}{\Lambda}\phi' - \left[(\theta' + 1)^2 + \frac{3}{\kappa}\cos^2\theta\right]\sin\phi\cos\phi + \frac{Q_\phi}{m^*\Lambda^2 L_r^2\dot{\nu}^2}, \tag{28}$$

$$\Lambda'' = \frac{2e\sin\nu}{\kappa}\Lambda' - \frac{(2m_1 - m)\frac{m_t}{2}}{m_1(m_2 + m_t)}\frac{\Lambda'^2}{\Lambda} + \left(\frac{m_2 + \frac{m_t}{2}}{m_2 + m_t}\right)\Lambda\left[\phi'^2 + (\theta' + 1)^2\cos^2\phi + \frac{1}{\kappa}\left(3\cos^2\theta\cos^2\phi - 1\right)\right] - \frac{T}{m_1\dot{\nu}^2 L_r(m_2 + m_t)/m} \tag{29}$$

where ν is the orbit true anomaly, e is the orbit eccentricity, $\Lambda = l/L$ is the nondimensional tether length, $\kappa = 1 + e\cos\nu$, L_r is a reference tether length, T is the tether tension, and $()' = \mathrm{d}()/\mathrm{d}\nu$. The generalized forces Q_θ and Q_ϕ are due to distributed forces along the tether, which are typically assumed to be negligible. The contributions due to aerodynamic drag are defined in Sect. 3.2.5.1.

2.2 Inelastic flexible tether model

More sophisticated models for tethered satellite systems treat the full effects of tether elasticity and flexibility. Examples include models based on discretization by assumed modes [20] or discretization by lumped masses [21]. In a typical lumped mass model, the tether is discretized into a series of point masses connected by elastic springs. The tension in each element can be computed explicitly based on the positions of the adjacent lumped masses. It is well known that the equations of motion for the system are 'stiff,' referring to the fact that the dynamics occur over very different timescales, requiring small integration step sizes to capture the very high frequency modes. For a tethered satellite system, the high frequency modes are the longitudinal elastic modes, followed by the string modes of the tether, libration modes, and finally the orbital motion. For short duration missions or analysis, the longitudinal modes are unlikely to have much significant effect on the overall motion (provided the tether remains taut). Thus, in this model the effects of longitudinal vibrations are ignored, and the tether is divided into a series of point masses connected via inelastic links. The geometric shortening of the distance to the tether tip is accounted for due to the changes in geometry of the system, but stretching of the tether is not. The degree of approximation is controlled by the number of discretized elements that are used.

The tether is modeled as consisting of a series of n point masses connected via inelastic links, as shown in Fig. 2. The (x, y, z) coordinate system rotates at the orbit angular velocity and is assumed to be attached at the center of mass of the orbit (mother satellite). Although not a necessary assumption in the model, it is assumed that the orbit of the mother satellite is prescribed and remains Keplerian. In general, this coordinate system would orbit in a plane defined by the classical orbital elements(Ω, i, ϖ). In the presence of a Newtonian gravitational field, the orientation of the orbital plane does not affect the system dynamics. However, it does affect any aerodynamic or electrodynamic forces due to the nature of the Earth's rotating atmosphere and magnetic field.

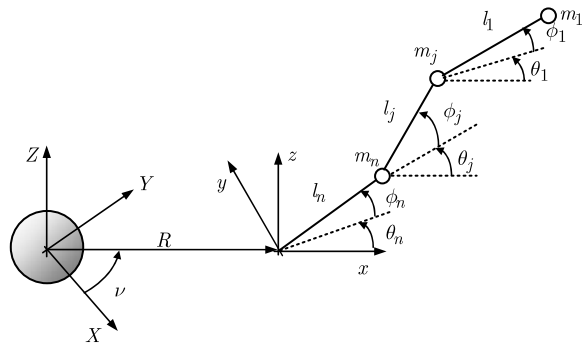

Fig. 2 Discretized flexible tether model

The acceleration of a mass in the rotating frame is given by

$$\ddot{\mathbf{r}} = \left(\ddot{x} - \dot{\omega}y - 2\omega\dot{y} - \omega^2 x\right)\mathbf{i} + \left(\ddot{y} + \dot{\omega}x + 2\omega\dot{x} - \omega^2 y\right)\mathbf{j} + \ddot{z}\mathbf{k} \tag{30}$$

where $\omega = \kappa^2\sqrt{\mu/p^3}$ is the orbital angular velocity, $p = a(1 - e^2)$ is the semilatus rectum, μ is the Earth's gravitational parameter, and a is the orbit semimajor axis. The contribution of forces due to the gravity-gradient is given by

$$\mathbf{F}_j^g = 2m_j\frac{\mu x_j}{R^3}\mathbf{i} - m_j\frac{\mu y_j}{R^3}\mathbf{j} - m_j\frac{\mu z_j}{R^3}\mathbf{k} = 2m_j\frac{\omega^2 x_j}{\kappa}\mathbf{i} - m_j\frac{\omega^2 y_j}{\kappa}\mathbf{j} - m_j\frac{\omega^2 z_j}{\kappa}\mathbf{k}. \tag{31}$$

Note that in (30), the contributions due to the center of mass motion R and corresponding true anomaly ν are canceled with the Newtonian gravity terms for the system center of mass. This is valid if the system is assumed to be in a Keplerian orbit.

Define the tension vector in the jth segment as

$$\mathbf{T}_j = T_j(\cos\theta_j \cos\phi_j \mathbf{i} + \sin\theta_j \cos\phi_j \mathbf{j} + \sin\phi_j \mathbf{k}). \tag{32}$$

Also, define the jth mass in terms of the generalized coordinates,

$$x_j = \sum_{k=j}^{n} l_k \cos\theta_k \cos\phi_k, \tag{33}$$

$$y_j = \sum_{k=j}^{n} l_k \sin\theta_k \cos\phi_k, \tag{34}$$

$$z_j = \sum_{k=j}^{n} l_k \sin\phi_k. \tag{35}$$

The tension forces on the jth mass are given by

$$\mathbf{F}_j^{\text{tension}} := \begin{cases} \mathbf{T}_{j-1} - \mathbf{T}_j, & 1 < j \le n, \\ -\mathbf{T}_j, & j = 1. \end{cases} \tag{36}$$

The equations of motion can be expressed in component form as

$$\begin{aligned} &\ddot{x}_j - \dot{\omega} y_j - 2\omega \dot{y}_j - \omega^2 x_j - 2\frac{\omega^2}{\kappa} x_j = \frac{F_j^x}{m_j}, \\ &\ddot{y}_j + \dot{\omega} x_j + 2\omega \dot{x}_j - \omega^2 y_j + \frac{\omega^2}{\kappa} y_j = \frac{F_j^y}{m_j}, \\ &\ddot{z}_j + \frac{\omega^2}{\kappa} z_j = \frac{F_j^z}{m_j} \end{aligned} \tag{37}$$

where m_j is the mass of the jth cable mass, and (F_j^x, F_j^y, F_j^z) is the vector of external forces acting on the jth mass in the orbital frame. Substitution of (33) through (35) into (37) gives the governing equations of motion in spherical coordinates. The equations of motion may be decoupled by employing a matrix transformation and forward substitution of the results. By multiplying the vector of (37) by the matrix

$$[C_j] = \begin{bmatrix} -\sin\theta_j & \cos\theta_j & 0 \\ -\cos\theta_j \sin\phi_j & -\sin\theta_j \sin\phi_j & \cos\phi_j \\ \cos\theta_j \cos\phi_j & \sin\theta_j \cos\phi_j & \sin\phi_j \end{bmatrix} \tag{38}$$

the general decoupled equations of motion can be expressed as

$$\begin{aligned} \ddot{\theta}_j = {} & -\dot{\omega} + 2(\dot{\theta}_j + \omega)\left[\dot{\phi}_j \tan\phi_j - \frac{\dot{l}_j}{l_j}\right] \\ & - 3\frac{\omega^2}{\kappa} \sin\theta_j \cos\theta_j \\ & - \frac{T_{j-1} \sin\theta_j \cos\theta_{j-1} \cos\phi_{j-1}}{m_j l_j \cos\phi_j} \\ & - \frac{F_j^x \sin\theta_j}{m_j l_j \cos\phi_j} + \frac{T_{j-1} \cos\theta_j \sin\theta_{j-1} \cos\phi_{j-1}}{m_j l_j \cos\phi_j} \\ & + \frac{T_{j+1} \cos\theta_j \sin\theta_{j+1} \cos\phi_{j+1}}{m_{j+1} l_j \cos\phi_j} \\ & - \frac{T_{j+1} \sin\theta_j \cos\theta_{j+1} \cos\phi_{j+1}}{m_{j+1} l_j \cos\phi_j} + \frac{F_j^y \cos\theta_j}{m_j l_j \cos\phi_j} \\ & + \frac{F_{j+1}^x \sin\theta_j}{m_{j+1} l_j \cos\phi_j} - \frac{F_{j+1}^y \cos\theta_j}{m_{j+1} l_j \cos\phi_j}, \end{aligned} \tag{39}$$

$$\begin{aligned} \ddot{\phi}_j = {} & -2\frac{\dot{l}_j}{l_j}\dot{\phi}_j \\ & - \left[(\dot{\theta}_j + \omega)^2 + \frac{3\omega^2 \cos^2\theta_j}{\kappa}\right] \sin\phi_j \cos\phi_j \\ & + \frac{T_{j-1}}{m_j l_j}(\cos\phi_j \sin\phi_{j-1} \\ & - \cos\theta_j \sin\phi_j \cos\theta_{j-1} \cos\phi_{j-1} \\ & - \sin\theta_j \sin\phi_j \sin\theta_{j-1} \cos\phi_{j-1}) \\ & + \frac{T_{j+1}}{m_{j+1} l_j}(\cos\phi_j \sin\phi_{j+1} \\ & - \cos\theta_j \sin\phi_j \cos\theta_{j+1} \cos\phi_{j+1} \\ & - \sin\theta_j \sin\phi_j \sin\theta_{j+1} \cos\phi_{j+1}) \\ & + \frac{F_j^z \cos\phi_j}{m_j l_j} - \frac{F_{j+1}^z \cos\phi_j}{m_{j+1} l_j} \\ & + \frac{F_{j+1}^y \sin\theta_j \sin\phi_j}{m_{j+1} l_j} \\ & - \frac{F_j^y \sin\theta_j \sin\phi_j}{m_j l_j} - \frac{F_j^x \cos\theta_j \sin\phi_j}{m_j l_j} \\ & + \frac{F_{j+1}^x \cos\theta_j \sin\phi_j}{m_{j+1} l_j}, \end{aligned} \tag{40}$$

$$\begin{aligned} \ddot{l}_j = {} & l_j\left[(\dot{\theta}_j + \omega)^2 \cos^2\phi_j + \dot{\phi}_j^2 \right. \\ & \left. - \frac{\omega^2}{\kappa}\left(1 - 3\cos^2\theta_j \cos^2\phi_j\right)\right] - \frac{T_j}{m_j} - \frac{T_j}{m_{j+1}} \\ & + \frac{F_j^z \sin\phi_j}{m_j} - \frac{F_{j+1}^z \sin\phi_j}{m_{j+1}} + \frac{F_j^y \sin\theta_j \cos\phi_j}{m_j} \end{aligned}$$

$$
\begin{aligned}
&- \frac{F_{j+1}^{y} \sin\theta_j \cos\phi_j}{m_{j+1}} + \frac{F_j^{x} \cos\theta_j \cos\phi_j}{m_j} \\
&- \frac{F_{j+1}^{x} \cos\theta_j \cos\phi_j}{m_{j+1}} \\
&+ \frac{T_{j-1}}{m_j}[\cos\theta_j \cos\phi_j \cos\theta_{j-1} \cos\phi_{j-1} \\
&+ \sin\phi_j \sin\phi_{j-1} \\
&+ \sin\theta_j \cos\phi_j \sin\theta_{j-1} \cos\phi_{j-1}] \\
&+ \frac{T_{j+1}}{m_{j+1}}[\cos\theta_j \cos\phi_j \cos\theta_{j+1} \cos\phi_{j+1} \\
&+ \sin\phi_j \sin\phi_{j+1} \\
&+ \sin\theta_j \cos\phi_j \sin\theta_{j+1} \cos\phi_{j+1}]. \qquad (41)
\end{aligned}
$$

These equations may be nondimensionalized by utilizing the following relationships

$$
\frac{\mathrm{d}}{\mathrm{d}t} = \omega \frac{\mathrm{d}}{\mathrm{d}\nu}, \qquad \frac{\mathrm{d}^2}{\mathrm{d}t^2} = \dot{\omega}\frac{\mathrm{d}}{\mathrm{d}\nu} + \omega^2 \frac{\mathrm{d}^2}{\mathrm{d}\nu^2}, \qquad (42)
$$

$$
l_j = \Lambda_j L, \qquad u_j = \frac{T_j}{m_j \omega^2 L}, \qquad (43)
$$

$$
\dot{\omega} = -2\frac{\omega^2}{\kappa} e \sin\nu. \qquad (44)
$$

Thus, the following nondimensional equations of motion are obtained

$$
\begin{aligned}
\theta_j'' = {} & 2(\theta_j' + 1)\left[\frac{e\sin\nu}{\kappa} + \phi_j' \tan\phi_j - \frac{\Lambda_j'}{\Lambda_j}\right] \\
& - \frac{3}{\kappa}\sin\theta_j \cos\theta_j \\
& - \frac{m_{j-1}}{m_j}\frac{u_{j-1}\sin\theta_j \cos\theta_{j-1}\cos\phi_{j-1}}{\Lambda_j \cos\phi_j} \\
& + \frac{m_{j-1}}{m_j}\frac{u_{j-1}\cos\theta_j \sin\theta_{j-1}\cos\phi_{j-1}}{\Lambda_j \cos\phi_j} \\
& + \frac{u_{j+1}\cos\theta_j \sin\theta_{j+1}\cos\phi_{j+1}}{\Lambda_j \cos\phi_j} \\
& - \frac{u_{j+1}\sin\theta_j \cos\theta_{j+1}\cos\phi_{j+1}}{\Lambda_j \cos\phi_j} \\
& + \frac{F_j^{y}\cos\theta_j}{m_j \omega^2 L \Lambda_j \cos\phi_j} \\
& - \frac{F_j^{x}\sin\theta_j}{m_j \omega^2 L \Lambda_j \cos\phi_j} + \frac{F_{j+1}^{x}\sin\theta_j}{m_{j+1}\omega^2 L \Lambda_j \cos\phi_j} \\
& - \frac{F_{j+1}^{y}\cos\theta_j}{m_{j+1}\omega^2 L \Lambda_j \cos\phi_j}, \qquad (45)
\end{aligned}
$$

$$
\begin{aligned}
\phi_j'' = {} & 2\frac{e\sin\nu}{\kappa}\phi' - 2\frac{\Lambda_j'}{\Lambda_j}\phi_j' \\
& - \left[(\theta_j' + 1)^2 + \frac{3\cos^2\theta_j}{\kappa}\right]\sin\phi_j \cos\phi_j \\
& + \frac{m_{j-1}}{m_j}\frac{u_{j-1}}{\Lambda_j}(\cos\phi_j \sin\phi_{j-1} \\
& - \cos\theta_j \sin\phi_j \cos\theta_{j-1}\cos\phi_{j-1} \\
& - \sin\theta_j \sin\phi_j \sin\theta_{j-1}\cos\phi_{j-1}) \\
& + \frac{u_{j+1}}{\Lambda_j}(\cos\phi_j \sin\phi_{j+1} \\
& - \cos\theta_j \sin\phi_j \cos\theta_{j+1}\cos\phi_{j+1} \\
& - \sin\theta_j \sin\phi_j \sin\theta_{j+1}\cos\phi_{j+1}) \\
& + \frac{F_j^{z}\cos\phi_j}{m_j\omega^2 L\Lambda_j} - \frac{F_{j+1}^{z}\cos\phi_j}{m_{j+1}\omega^2 L\Lambda_j} \\
& + \frac{F_{j+1}^{y}\sin\theta_j \sin\phi_j}{m_{j+1}\omega^2 L\Lambda_j} \\
& - \frac{F_j^{y}\sin\theta_j \sin\phi_j}{m_j\omega^2 L\Lambda_j} - \frac{F_j^{x}\cos\theta_j \sin\phi_j}{m_j\omega^2 L\Lambda_j} \\
& + \frac{F_{j+1}^{x}\cos\theta_j \sin\phi_j}{m_{j+1}\omega^2 L\Lambda_j}, \qquad (46)
\end{aligned}
$$

$$
\begin{aligned}
\Lambda_j'' = {} & 2\frac{e\sin\nu}{\kappa}\Lambda_j' \\
& + \Lambda_j\left[(\theta_j' + 1)^2\cos^2\phi_j + \phi_j'^2\right. \\
& \left. - \frac{1}{\kappa}\left(1 - 3\cos^2\theta_j \cos^2\phi_j\right)\right] - u_j - \frac{m_j}{m_{j+1}}u_j \\
& + \frac{F_j^{z}\sin\phi_j}{m_j\omega^2 L} - \frac{F_{j+1}^{z}\sin\phi_j}{m_{j+1}\omega^2 L} + \frac{F_j^{y}\sin\theta_j \cos\phi_j}{m_j\omega^2 L} \\
& - \frac{F_{j+1}^{y}\sin\theta_j \cos\phi_j}{m_{j+1}\omega^2 L} + \frac{F_j^{x}\cos\theta_j \cos\phi_j}{m_j\omega^2 L} \\
& - \frac{F_{j+1}^{x}\cos\theta_j \cos\phi_j}{m_{j+1}\omega^2 L} \\
& + \frac{m_{j-1}}{m_j}u_{j-1}[\cos\theta_j \cos\phi_j \cos\theta_{j-1}\cos\phi_{j-1} \\
& + \sin\phi_j \sin\phi_{j-1} \\
& + \sin\theta_j \cos\phi_j \sin\theta_{j-1}\cos\phi_{j-1}]
\end{aligned}
$$

$$
\begin{aligned}
&+ u_{j+1}[\cos\theta_j \cos\phi_j \cos\theta_{j+1} \cos\phi_{j+1} \\
&+ \sin\phi_j \sin\phi_{j+1} \\
&+ \sin\theta_j \cos\phi_j \sin\theta_{j+1} \cos\phi_{j+1}]. \qquad (47)
\end{aligned}
$$

Equations (45) through (47) utilize the orbit true anomaly ν as independent variable, and L is a scaling length representing the length of each tether element when fully deployed. The applicable boundary conditions are

$$
\begin{aligned}
&m_0 = 0, \qquad u_0 = 0, \\
&m_{n+1} = \infty, \qquad u_{n+1} = 0.
\end{aligned} \qquad (48)
$$

The equations (45) through (47) define the dynamics of the tethered satellite system using spherical coordinates. These are not as general as Cartesian coordinates due to the singularity introduced when $\phi_j = -\frac{\pi}{2}, \frac{\pi}{2}$. This represents very large out of plane librational motion or very large out of plane lateral motion. Although this is a limitation of the model, such situations need to be avoided for most practical missions.

2.2.1 *Variable length case*

The tether is modeled as a collection of lumped masses connected by inelastic links, which makes dealing with the case of a variable length tether more difficult than in the single link model. In particular, it is necessary to have a state vector of variable dimension and to add and subtract elements from the model at appropriate times. When the tether is treated as elastic, great care needs to be exercised to ensure that the introduction of new elements does not create unnecessary cable oscillations. This can happen if the position of the new mass results in the incorrect tension in the new element. However, for an inelastic tether, the introduction of a new mass occurs such that it is placed along the same line as the existing element. Thus, the new initial conditions for the incoming element are that it has the same angles and angle rates as the existing element (closest to the deployer). Alternative formulations based on the variation principle of Hamilton–Ostrogradski and which transform the deployed length to a fixed interval by means of a new spatial coordinate have also been used [19]. However, this was not considered in this work.

If the critical length for introduction of a new element is defined as $\Lambda^* \triangleq 1 + k^*$, then the new element is initialized with a length of k^* in nondimensional units, and the same length rate as the previous nth element. During retrieval, elements must be removed. Here, the nth element to be removed and the $(n-1)$th element need to be used to update the initial conditions for the new n^*th element. In this work, the position and velocity of the $(n-1)$th mass is used to initialize the n^*th element. Thus, let

$$
\begin{aligned}
x_{n-1} &= \Lambda_n \cos\theta_n \cos\phi_n + \Lambda_{n-1} \cos\theta_{n-1} \cos\phi_{n-1}, \\
y_{n-1} &= \Lambda_n \sin\theta_n \cos\phi_n \\
&\quad + \Lambda_{n-1} \sin\theta_{n-1} \cos\phi_{n-1}, \\
z_{n-1} &= \Lambda_n \sin\phi_n + \Lambda_{n-1} \sin\phi_{n-1}
\end{aligned} \qquad (49)
$$

from which

$$
\begin{aligned}
\Lambda_{n^*} &= \sqrt{x_{n-1}^2 + y_{n-1}^2 + z_{n-1}^2}, \\
\theta_{n^*} &= \operatorname{atan2}(y_{n-1}, x_{n-1}), \\
\phi_{n^*} &= \sin^{-1}(z_{n-1}/\Lambda_{n^*})
\end{aligned} \qquad (50)
$$

where atan2 represents the four quadrant inverse tangent where the usual arctangent is defined by $\tan^{-1}(\frac{y_{n-1}}{x_{n-1}})$. Similarly, the relative velocity of the $(n-1)$th mass in the rotating frame is given by

$$
\begin{aligned}
x'_{n-1} &= \Lambda'_n \cos\theta_n \cos\phi_n - \Lambda_n \theta'_n \sin\theta_n \cos\phi_n \\
&\quad - \Lambda_n \phi'_n \cos\theta_n \sin\phi_n \\
&\quad + \Lambda'_{n-1} \cos\theta_{n-1} \cos\phi_{n-1} \\
&\quad - \Lambda_{n-1} \theta'_{n-1} \sin\theta_{n-1} \cos\phi_{n-1} \\
&\quad - \Lambda_{n-1} \phi'_{n-1} \cos\theta_{n-1} \sin\phi_{n-1}, \\
y'_{n-1} &= \Lambda'_n \sin\theta_n \cos\phi_n + \Lambda_n \theta'_n \cos\theta_n \cos\phi_n \\
&\quad - \Lambda_n \phi'_n \sin\theta_n \sin\phi_n \\
&\quad + \Lambda'_{n-1} \sin\theta_{n-1} \cos\phi_{n-1} \\
&\quad + \Lambda_{n-1} \theta'_{n-1} \cos\theta_{n-1} \cos\phi_{n-1} \\
&\quad - \Lambda_{n-1} \phi'_{n-1} \sin\theta_{n-1} \sin\phi_{n-1}, \\
z'_{n-1} &= \Lambda'_n \sin\phi_n + \Lambda_n \phi'_n \cos\phi_n + \Lambda'_{n-1} \sin\phi_{n-1} \\
&\quad + \Lambda_{n-1} \phi'_{n-1} \cos\phi_{n-1}
\end{aligned} \qquad (51)
$$

from which

$$
\begin{aligned}
\Lambda'_{n^*} &= x'_{n-1} \cos\phi_{n^*} \cos\theta_{n^*} + y'_{n-1} \cos\phi_{n^*} \sin\theta_{n^*} \\
&\quad + z'_{n-1} \sin\phi_{n^*},
\end{aligned}
$$

$$\theta'_{n^*} = (y'_{n-1}\cos\theta_{n^*} - x'_{n-1}\sin\theta_{n^*}) /(\Lambda_{n^*}\cos\phi_{n^*}), \quad (52)$$

$$\phi'_{n^*} = (z'_{n-1}\cos\phi_{n^*} - x'_{n-1}\sin\phi_{n^*}\cos\theta_{n^*} - y'_{n-1}\sin\phi_{n^*}\sin\theta_{n^*})/\Lambda_{n^*}.$$

It should be noted that these updates keep the position and velocity of the $(n-1)$th mass the same across the update. The reason for this is that the positions and velocities of all subsequent masses depend on the position/velocity of the nth mass. Hence, if this is changed, then the position and velocity of all masses representing the tether change instantaneously. The accuracy of the updates depend on the transition parameter k^{**}, which is used to monitor the length of the nth segment. An element is removed when $\Lambda_n < k^{**}$. Because the tether is inelastic, altering the length of the new nth element does not keep the total tether length or mass constant unless the nth and $(n-1)$th elements are tangential. Therefore, by choosing k^{**} small enough, the errors in the approximation can be made small.

2.3 Tension determination

2.3.1 Tension control case

For control purposes, it is assumed that the level of tension in the tether is controlled. Thus, u_n is specified or determined through a control law. This means that the nth element is allowed to vary in length according to the applied tension, but all other segments remained fixed in length. The problem is to then solve for the remaining unknown tension constraints that enforce constant total length of the remaining segments. Once these are known, they are back-substituted into (45) and (46), as well as (47) for the nth element. The equations formed by the set (47) are linear in the tensions u_j, and can thus be solved using standard techniques. This assumes that the segment lengths, length rates, and length accelerations are specified. Note that the equation for the nth element is not used in this process. In this work, LAPACK is utilized in solving the simultaneous equations.

2.3.2 Fixed length case

To simulate the case of a fixed length tether, (47) are set to zero for $j = 1, \ldots, n$, allowing the unknown tensions u_j, $j = 1, \ldots, n$ to be determined. The resulting tensions are substituted back into the librational dynamics to determine the evolution of the system dynamics.

3 Optimal deployment control

The main reason for posing the deployment/retrieval problem as an optimal control problem is that it is inherently already a two-point boundary value problem. That is, the trajectory designer usually knows what the state of the system should be at the beginning of deployment (i.e., the ejection parameters), and knows what the state of the system should be at the end of the deployment phase. For many missions, the tether must be deployed to the local vertical, which is a stable equilibrium position for circular orbits. The problem thereafter is *how* to deploy the tether between the initial state and the terminal state. This depends largely on the system constraints, but recent work shows that the selection of the performance index is often crucial to obtaining satisfactory deployment performance [5]. For instance, a minimum time deployment results in a bang-bang control tension—clearly unacceptable for a flexible, elastic system where one of the key requirements is to keep the tether from becoming slack.

Optimal control is typically approached from two directions. The first is to view the problem in the dual space formed by the states and costates by application of the Pontryagin Maximum Principle (PMP). Unless the problem is simple and has an analytic solution, then some kind of discretization is inevitable in obtaining an approximate solution. The alternative and quicker approach is to view the problem in a discrete space before applying criteria for optimality (typically, the Kuhn–Karush–Tucker (KKT) conditions). Both the PMP and KKT conditions effectively transform the original problem into a dual space. If the discretization schemes are chosen properly, it can be shown that the resulting necessary conditions can be made equivalent. That is, the discretized PMP conditions are identical to the KKT conditions of the discretized problem [22]. The practical importance of these developments is that difficult and complex problems can be solved relatively easily with little labor. The methods that are used to solve optimal control problems in this way are often termed direct transcription methods, but it must be pointed out that not all discretization methods commute the operations of dualization and discretization.

One of the most powerful methods available that does so is the Legendre pseudospectral method [23, 24].

3.1 Direct transcription techniques

Consider the problem of finding the state-control pair $\{\mathbf{x}(t), \mathbf{u}(t)\}$ that minimize the performance index

$$\mathcal{J} = \mathcal{E}\big[\mathbf{x}(t_f), t_f\big] + \int_{t_0}^{t_f} \mathcal{L}\big[\mathbf{x}(t), \mathbf{u}(t), t\big]\,\mathrm{d}t \tag{53}$$

subject to the nonlinear state equations

$$\dot{\mathbf{x}}(t) = \mathbf{f}(\mathbf{x}(t), \mathbf{u}(t), t) \tag{54}$$

the end point conditions

$$\mathbf{e}_L^0 \le \mathbf{e}\big[\mathbf{x}(t_0), t_0\big] \le \mathbf{e}_U^0, \tag{55}$$

$$\mathbf{e}_L^f \le \mathbf{e}\big[\mathbf{x}(t_f), t_f\big] \le \mathbf{e}_U^f \tag{56}$$

path constraints

$$\mathbf{g}_L \le \mathbf{g}\big[\mathbf{x}(t), \mathbf{u}(t), t\big] \le \mathbf{g}_U \tag{57}$$

and box constraints

$$\mathbf{x}_L \le \mathbf{x}(t) \le \mathbf{x}_U, \qquad \mathbf{u}_L \le \mathbf{u}(t) \le \mathbf{u}_U \tag{58}$$

where $\mathbf{x} \in \mathbb{R}^{n_x}$ are the state variables, $\mathbf{u} \in \mathbb{R}^{n_u}$ are the control inputs, $t \in \mathbb{R}$ is the time, $\mathcal{E} : \mathbb{R}^{n_0} \times \mathbb{R} \to \mathbb{R}$ is the Mayer cost function, $\mathcal{L} : \mathbb{R}^{n_x} \times \mathbb{R}^{n_u} \times \mathbb{R} \to \mathbb{R}$ is the integrand of the Bolza cost function, $\mathbf{e}_L^0 \in \mathbb{R}^{n_x} \times \mathbb{R} \to \mathbb{R}^{n_0}$ and $\mathbf{e}_U^0 \in \mathbb{R}^{n_x} \times \mathbb{R} \to \mathbb{R}^{n_0}$ are the lower and upper bounds on the initial point conditions, $\mathbf{e}_L^f \in \mathbb{R}^{n_x} \times \mathbb{R} \to \mathbb{R}^{n_f}$ and $\mathbf{e}_U^f \in \mathbb{R}^{n_x} \times \mathbb{R} \to \mathbb{R}^{n_f}$ are the lower and upper bounds on the final point conditions, and $\mathbf{g}_L \in \mathbb{R}^{n_x} \times \mathbb{R}^{n_u} \times \mathbb{R} \to \mathbb{R}^{n_g}$ and $\mathbf{g}_U \in \mathbb{R}^{n_x} \times \mathbb{R}^{n_u} \times \mathbb{R} \to \mathbb{R}^{n_g}$ are the lower and upper bounds on the path constraints.

A general reusable software package for solving single (and multiple)-phase optimal control problems called DIRECT [25] has been developed by the author. The package utilizes the MATLAB environment to formulate the cost function, state equations, boundary conditions, and path constraints. The problem is automatically converted into an appropriate NLP depending on the selected discretization method for the differential equations. The NLP is solved using the sparse sequential quadratic programming software SNOPT [26], originally coded in Fortran, but called from MATLAB via a mex-file interface.

3.2 Evolutionary optimization of flexible tether trajectories

One of the current drawbacks of the direct transcription scheme is that it relies on a discretization of both the state and control trajectories. This is, in fact, what makes it so robust for most problems. However, for multibody systems, it becomes more and more difficult to apply effectively as the degree of dimensionality of the system grows. This is even more apparent when one considers the tether as modeled as a collection of lumped masses. Changes in length call for a variable state dimension, necessitating multiple phases [27]. The difficulty lies in the fact that direct transcription methods are intended for systems with relatively low dimensionality without significant changes in the state dimension.

In this paper, a direct shooting method is developed with application to tethered satellite systems. Direct shooting, in contrast to direct transcription, only discretizes the control inputs and relies on explicit propagation of the state trajectories by means of a high-order integrator, such as a Runge–Kutta algorithm. One of the problems with this approach has been that the system is often sensitive to small changes in the control inputs near the beginning of the trajectory, and hence explicit propagation can cause numerical difficulties and often divergence. To overcome this, previous knowledge about optimal trajectories for tethered satellites is combined with more robust optimization methods to enhance the solution accuracy while reducing the number of decision variables representing the control input.

3.2.1 Discretization of length history

Consider the problem of deploying/retrieving a tether from some given initial length and length rate, $\Lambda_0 = \Lambda(\nu_0)$, $\Lambda_0' = \Lambda'(\nu_0)$, to some final length and length rate, $\Lambda_f = \Lambda(\nu_f)$, $\Lambda_f' = \Lambda'(\nu_f)$. In [5], it was shown that by minimizing the square of the tether length acceleration, very smooth trajectories that result in slow changing tether tensions are produced. Hence, we can approximate the variation in length over the trajectory by means of Chebyshev polynomials as follows

$$\Lambda_n(\tau) \cong \frac{a_0}{2} + \sum_{k=1}^{n} a_k \mathcal{T}_k(\tau) \tag{59}$$

where $\tau \in [-1, 1]$ so that

$$\nu = (\nu_f - \nu_0)\tau/2 + (\nu_f + \nu_0)/2 \tag{60}$$

and $a_k, k = 0, \ldots, n$ are the series coefficients. One approach is to treat the a_k coefficients as unknowns to be optimized directly. The problem with this is that the coefficients themselves do not have an intuitive physical meaning. Therefore, it is difficult to devise initial guesses for them and to provide appropriate bounds on their variation. Instead, we take advantage of the fact that we know that the second derivative of (59) should be minimized over the trajectory

$$J = \int_{-1}^{1} (\ddot{\Lambda}_n)^2 \, \mathrm{d}\tau \tag{61}$$

where $\dot{(\,)} = \mathrm{d}(\,)/\mathrm{d}\tau$. It should be noted that the physical length acceleration requires a transformation metric that is derived via (60). However, because this is an affine transformation, it does not matter in which domain the length acceleration is minimized. Using (59) we have

$$\begin{aligned} \dot{\Lambda}_n(\tau) &= \sum_{k=1}^{n} a_k \dot{\mathcal{T}}_k(\tau), \\ \ddot{\Lambda}_n(\tau) &= \sum_{k=1}^{n} a_k \ddot{\mathcal{T}}_k(\tau) \end{aligned} \tag{62}$$

and $\Lambda'_n = 2\dot{\Lambda}_n/(\nu_f - \nu_0)$, $\Lambda''_n = 4\ddot{\Lambda}_n/(\nu_f - \nu_0)^2$. To (61) we append the desired boundary conditions by means of Lagrange multipliers. In addition to the boundary conditions, additional interior point constraints are introduced that dictate the internal shape of the trajectory. For example

$$\Lambda(\tau_j) = \Lambda_j, \quad j = 1, \ldots, n_i \tag{63}$$

and τ_j, $j = 1, \ldots, n_i$ are a set of preassigned nodes. The nodes could be defined by the Chebyshev–Gauss–Lobatto points or Chebyshev–Gauss points if desired. However, here they are chosen to be equally spaced. Hence, the augmented cost becomes

$$\begin{aligned} \bar{J} = J &+ \lambda_0\big[\Lambda_n(-1) - \Lambda_0\big] + \lambda_1\big[\Lambda'_n(-1) - \Lambda'_0\big] \\ &+ \lambda_2\big[\Lambda_n(1) - \Lambda_f\big] + \lambda_3\big[\Lambda'_n(1) - \Lambda'_f\big] \\ &+ \sum_{j=1}^{n_i} \lambda_{3+j}\big[\Lambda_n(\tau_j) - \Lambda_j\big] \\ &+ \lambda_{4+n_i}\big[\Lambda''_n(1) - \Lambda''_f\big] \end{aligned} \tag{64}$$

where λ_j are the set of Lagrange multipliers. Note that an additional boundary condition for the length acceleration of the tether at the final time is also specified. This would typically be zero. In order to ensure a solution, n must be selected such that $n > n_i + 5$. The larger the value of n, the smoother the resulting trajectory will be. The unknown coefficients a_k and the Lagrange multipliers are determined by taking partial derivatives of (64) with respect to each parameter. This results in a set of linear algebraic equations for the unknowns, which can be solved analytically. These solutions can be substituted back into (59) to obtain an explicit solution for the optimal variation in length given a set of boundary conditions and interior point constraints. By keeping these values in symbolic form, it is easy to obtain different solutions as a function of these variables.

3.2.2 *Tension control*

The variation in length given by (59) is not the actual variation in length of the tether when it is controlled using tension control. This is due to the fact that tension control affects the system dynamically rather than kinematically. To translate the desired variation in tether length given by (59) into a tension control input, (29) is used as a basis for developing a length tracking tension control law as follows

$$\begin{aligned} T_c = &\big[\Lambda''_0 - \Lambda''_c + k_1(\Lambda - \Lambda_c) + k_2(\Lambda' - \Lambda'_c)\big] \\ &\times m_1 \dot{\nu}^2 L(m_2 + m_t)/m \end{aligned} \tag{65}$$

where

$$\begin{aligned} \Lambda''_0 = &\frac{2e \sin \nu}{\kappa} \Lambda' - \frac{(2m_1 - m)\frac{m_t}{2}}{m_1(m_2 + m_t)} \frac{\Lambda'^2}{\Lambda} \\ &+ \left(\frac{m_2 + \frac{m_t}{2}}{m_2 + m_t}\right) \Lambda \bigg[\phi'^2 + (\theta' + 1)^2 \cos^2 \phi \\ &+ \frac{1}{\kappa}\big(3 \cos^2 \theta \cos^2 \phi - 1\big)\bigg]. \end{aligned} \tag{66}$$

Note the distinction between the actual tether length Λ and the commanded value Λ_c. The subscript c refers to the commanded value of the variable.

3.2.3 *Constraints*

Typically in trajectory design for tethered satellites, it is important to observe a number of constraints related to the control input. For instance, it is well-known that slack or very low tension tethers can be

problematic in space because control over the subsatellite motion is lost. Furthermore, it is almost impossible to predict the motion of a slack tether due to shape memory effects from the tether being stored on a drum prior to deployment. When a tether transitions from slack to taut, it is often accompanied by large oscillations in the string modes and longitudinal modes. Due to the lack of damping transverse to the tether motion, it can be difficult to recover from the ensuing vibrations. For this reason, it is important to keep the tension 'large' during deployment. This is achieved indirectly by minimizing the length acceleration, but a minimum tension constraint is often also required. In this case, the tension is applied according to

$$T_d = \begin{cases} T_c, & T_c > T_{\min}, \\ T_{\min}, & T_c \le T_{\min}. \end{cases} \tag{67}$$

Another important constraint that will be considered in the example used in this paper is that certain deployers are designed for deployment-only. That is, a friction brake is used to slow or speed up the deployment depending on the number of times the tether is wrapped around the friction pole. Because of this, the tether deployment cannot be reversed. Although one can enforce the constraint in the control design, it is possible for the simulator to actually pull some of the tether in due to the dynamic control. Thus, the actual tension needs to be modified according to

$$T = \begin{cases} T_d, & \dot{l} \ge 0, \\ [\Lambda_0'' + k_3 \Lambda'] m_1 \dot{\nu}^2 L(m_2 + m_t)/m, & \dot{l} < 0. \end{cases} \tag{68}$$

Similar modifications can be made for maximum deployment/retrieval speeds and/or maximum tether lengths.

3.2.4 Evolutionary algorithms

To summarize, the optimal control problem is reduced to a parameter optimization problem involving only a small number of parameters specified in (64), $\Lambda(\tau_j) = \Lambda_j,\ j = 1, \ldots, n_i$. These parameters are selected to minimize or maximize another selected performance index. For example, for deployment of a flexible tether to the local vertical, the cost to be minimized might be selected as

$$\begin{aligned} \mathcal{J} = {} & w_1 \big[\theta_{\text{sub}}(\nu_f) - \theta_d\big]^2 + w_2 \big[\theta'_{\text{sub}}(\nu_f) - \theta'_d\big]^2 \\ & + w_3 \big[\phi_{\text{sub}}(\nu_f) - \phi_d\big]^2 + w_4 \big[\phi'_{\text{sub}}(\nu_f) - \phi'_d\big]^2 \\ & + w_5 \sum_{j=1}^{n} \big\{ \big[\theta''_j(\nu_f)\big]^2 + \big[\phi''_j(\nu_f)\big]^2 \big\} \end{aligned} \tag{69}$$

where the subscript sub refers to the subsatellite variables, the subscript d refers to the desired values, w_j are a set of constant weighting coefficients, ν_f is the true anomaly at the end of the deployment, and the final term in (69) essentially minimizes the final tether lateral vibrations because it minimizes the angular accelerations of all the tether segments. Numerical results show that merely minimizing the angles and angle rates does not guarantee that the tether will not librate after the termination of the deployment phase. It is possible for the angle and angle rate to be zero, but the acceleration to be nonzero at a particular instant of time. This is especially important when there may be aerodynamic drag acting on the tether. In this case, the tether will not remain straight and will not deploy to a zero libration angle. However, minimizing the final angular accelerations will minimize both the lateral vibrations and the final libration dynamics. If the cost is very small, then the tether will be deployed close to an equilibrium position. It should be noted, however, that for nonequatorial orbits and a rotating atmosphere, it is impossible for the tether to remain in equilibrium due to the changing direction of the drag forces.

To solve the aforementioned optimization problem, evolutionary algorithms such as genetic algorithms and simulated annealing are considered. Although these algorithms differ in methodology, they are both able to converge to global minimum solutions even if the starting guess is bad. In fact, no starting guesses are used in most cases and the initial parameters are selected randomly within the limits of the parameters. However, both approaches require tuning parameters to help convergence. For genetic algorithms, parameters such as the mutation rate, crossover probability, number of members of the population, etc., need to be chosen. For simulated annealing, the annealing temperature schedule is particularly important. Once solutions are obtained from these algorithms, they can be used as a starting guess for gradient-based optimization routines, such as quasi-Newton methods.

3.2.5 YES2 deployer example

As mentioned in the Introduction, this paper is motivated by the YES2 mission for which optimal trajectories are required for two phases. In this work, only the first phase is considered. This phase requires deployment of 3.5 km of tether to, or near to, the local vertical. A friction-brake is used to control the deployment with a given set of parameters. The ejection parameters for the subsatellite are specified, together with the orbital parameters and tether properties. The optimization task is to develop the deployment schedule in terms of the number of brake turns of the tether on the friction pole. The major factor which complicates the optimization is that the orbital altitude is reasonably low and the effects of aerodynamic drag on the tether become noticeable. The following subsections derive the aerodynamic force contributions to the tether.

3.2.5.1 Tether drag calculations The principle of virtual work is utilized to derive the generalized forces Q_θ and Q_ϕ. Because the effects of drag are distributed along the tether, it is necessary to calculate the integral of an elemental generalized force acting on the tether. However, this proves to be extremely difficult unless one assumes a simple atmospheric density profile. Therefore, a discretization of the tether is performed for computation of the total virtual work. The following numerical scheme is used to represent the various parts of the tether

$$x_j = \begin{cases} -r_1, & j = 1 \text{ (mass } m_1\text{)}, \\ \left(\frac{2j-3}{2n}\right)l - r_1, & j = 2, \ldots, n_e + 1 \text{ (tether)}, \\ r_2, & j = n_e + 2 \text{ (mass } m_2\text{)} \end{cases} \tag{70}$$

where $r_1 = (m_2 + m_t/2)l/m$ is the distance of the mother satellite from the center of mass, $r_2 = (m_1 + m_t/2)l/m$ is the distance of the payload from the center of mass, and n_e is the number of discrete elements used to model the forces on the tether.

The generalized forces for the system may be determined by summing the force contributions from each element in the system as

$$Q_\theta = \sum_{j=1}^{n_e+2} \mathbf{F}_j \cdot \frac{\partial \mathbf{R}_j}{\partial \theta}, \qquad Q_\phi = \sum_{j=1}^{n_e+2} \mathbf{F}_j \cdot \frac{\partial \mathbf{R}_j}{\partial \phi}. \tag{71}$$

The vector $\mathbf{R}_j$ is given by

$$\mathbf{R}_j = (R - x_j \cos\theta\cos\phi)\mathbf{i} - x_j \sin\theta\cos\phi\,\mathbf{j} + x_j \sin\phi\,\mathbf{k} \tag{72}$$

where $(\mathbf{i}, \mathbf{j}, \mathbf{k})$ are unit vectors in the rotating orbital frame, and R is the orbit radius to the system center of mass. The inertial velocity of the center of an element of tether in the rotating frame is given by

$$\begin{aligned} \mathbf{v}_j = {} & (\dot{R} - \dot{x}_j \cos\theta\cos\phi + x_j\dot{\theta}\sin\theta\cos\phi \\ & + x_j\dot{\phi}\cos\theta\sin\phi + \dot{\nu}x_j \sin\theta\cos\phi)\mathbf{i} \\ & + \big(-\dot{x}_j \sin\theta\cos\phi - x_j\dot{\theta}\cos\theta\cos\phi \\ & + x_j\dot{\phi}\sin\theta\sin\phi + \dot{\nu}[R - x_j\cos\theta\cos\phi]\big)\mathbf{j} \\ & + (\dot{x}_j \sin\phi + x_j\dot{\phi}\cos\phi)\mathbf{k} \end{aligned} \tag{73}$$

where the velocity of the end masses are calculated as

$$\dot{r}_1 = \frac{(m_2 + m_t)}{m}\dot{l}, \qquad \dot{r}_2 = \frac{m_1}{m}\dot{l} \tag{74}$$

so that

$$\dot{x}_j = \begin{cases} -\dot{r}_1, & j = 1 \text{ (mass } m_m\text{)}, \\ \dot{l} - \dot{r}_1 = \dot{r}_2, & j = 2, \ldots, n_e + 1 \text{ (tether)}, \\ \dot{r}_2, & j = n_e + 2 \text{ (mass } m_2\text{)}. \end{cases} \tag{75}$$

Note that (75) is derived on the basis of the tether being inextensible, i.e., all elements move uniformly. In the typical approximation of $m_m \to \infty$, $\dot{r}_m \to 0$ and all parts of the tether move at the deployment velocity.

The components of $\mathbf{R}_j$ in the inertial frame are obtained by the following transformation

$$\{X_j \quad Y_j \quad Z_j\}^T = [C]\mathbf{R}_j, \tag{76}$$

$$[C] = \begin{bmatrix} \mathrm{c}\Omega\mathrm{c}\psi - \mathrm{s}\Omega\mathrm{s}\psi\mathrm{c}i & -\mathrm{c}\Omega\mathrm{s}\psi - \mathrm{s}\Omega\mathrm{c}\psi\mathrm{c}i & \mathrm{s}\Omega\mathrm{s}i \\ \mathrm{s}\Omega\mathrm{c}\psi + \mathrm{c}\Omega\mathrm{s}\psi\mathrm{c}i & -\mathrm{s}\Omega\mathrm{s}\psi + \mathrm{c}\Omega\mathrm{c}\psi\mathrm{c}i & -\mathrm{c}\Omega\mathrm{s}i \\ \mathrm{s}\psi\mathrm{s}i & \mathrm{c}\psi\mathrm{s}i & \mathrm{c}i \end{bmatrix} \tag{77}$$

and c() and s() represent the cosine and sine functions, respectively, where $\psi = \varpi + \nu$, Ω is the longitude of the ascending node, i is the orbit inclination, and ϖ is the argument of perigee. The velocity of the atmosphere may be calculated by assuming that it rotates with the Earth,

$$\mathbf{v}_a = -\omega_e Y_j \mathbf{i} + \omega_e X_j \mathbf{j} \tag{78}$$

where ω_e is the angular rotation of the Earth. Hence, the relative velocity of an element of the tether system may be obtained in the orbital coordinate system as follows

$$\mathbf{v}_{\mathrm{rel},j} = \mathbf{v}_j - [C]^T \mathbf{v}_a. \tag{79}$$

After evaluating and simplifying (79), the following is obtained

$$\begin{aligned}\mathbf{v}_{\mathrm{rel},j} = {} & \big(\dot{R} - \dot{x}_j \cos\theta\cos\phi + x_j\dot{\theta}\sin\theta\cos\phi \\ & + x_j\dot{\phi}\cos\theta\sin\phi + \dot{\nu}x_j\sin\theta\cos\phi \\ & - \omega_e x_j \cos i \sin\theta\cos\phi \\ & - \omega_e x_j \sin i \cos(\omega+\nu)\sin\phi\big)\mathbf{i} \\ & + \big(-\dot{x}_j\sin\theta\cos\phi - x_j\dot{\theta}\cos\theta\cos\phi \\ & + x_j\dot{\phi}\sin\theta\sin\phi + \dot{\nu}[R - x_j\cos\theta\cos\phi] \\ & - \omega_e R\cos i + \omega_e x_j\cos i\cos\theta\cos\phi \\ & + \omega_e x_j \sin i\sin(\omega+\nu)\sin\phi\big)\mathbf{j} \\ & + \big(\dot{x}_j\sin\phi + x_j\dot{\phi}\cos\phi \\ & + \omega_e R\sin i\cos(\omega+\nu) \\ & - \omega_e x_j\sin i\cos(\omega+\nu)\cos\theta\cos\phi \\ & + \omega_e x_j\sin i\sin(\omega+\nu)\sin\theta\cos\phi\big)\mathbf{k}. \end{aligned} \tag{80}$$

A unit vector tangent to the tether is defined by

$$\mathbf{t} = -\cos\theta\cos\phi\mathbf{i} - \sin\theta\cos\phi\mathbf{j} + \sin\phi\mathbf{k}. \tag{81}$$

Hence, the component of the relative velocity tangent to the tether is obtained as

$$\mathbf{v}_{t,j} = (\mathbf{v}_{\mathrm{rel},j}\cdot\mathbf{t})\cdot\mathbf{t}. \tag{82}$$

The component of velocity normal to the tether is obtained as

$$\mathbf{v}_{n,j} = \mathbf{v}_{\mathrm{rel},j} - \mathbf{v}_{t,j}. \tag{83}$$

This finally leads to the computation of the drag force in the orbital frame

$$\mathbf{F}_j = -\frac{1}{2}\rho_j C_{D_j} A_j \mathbf{v}_{n,j}|\mathbf{v}_{n,j}| \tag{84}$$

where ρ_j is the atmospheric density, C_{D_j} is the tether drag coefficient, and A_j is the drag area. The drag on the payload and mother satellite are calculated assuming spherical bodies. The variation in atmospheric density is calculated using an analytical approximation

$$\begin{aligned}\rho_j = {} & \frac{1.47\times10^{-16}T_{\mathrm{ex}}(3000 - T_{\mathrm{ex}})}{(1+2.9[h_j/1000-200]/T_{\mathrm{ex}})^{10}} \\ & + \frac{0.032}{(h_j/1000+1200)^4}\end{aligned} \tag{85}$$

where T_{ex} is the exospheric temperature, and h_j is the altitude of the jth element.

For the flexible tether model, the drag forces are computed in a very similar way, except that the velocities normal to the tether at each individual cable element are used. Because the tether is flexible, each element is no longer tangential to the subsatellite line. Furthermore, half of the drag forces from the segments adjacent to each mass are applied to each individual mass. For the flexible model, the applied forces are the Cartesian components of the forces in the orbital coordinate system. Similar conversions to and from the inertial system are required as in (76).

3.2.5.2 Deployer parameters The tether braking mechanism is modeled after the SEDS deployer, which uses a friction brake to control the speed of the tether deployment. The force applied to the tether due to braking is given by [17]

$$\begin{aligned}T = {} & \big(T_0 + I\rho\dot{l}^2[1 - A_{\mathrm{sol}}l/L_{\mathrm{ref}}]^{-E}\big) \\ & \times \exp\big(f_\theta|\theta-\theta_0|\big)\exp\big(2\pi f_n n^*\big)\end{aligned} \tag{86}$$

where T_0 (0.01 N) is the minimal tension due to friction, I (3.1) is the inertia multiplier, ρ (0.000185 kg/m) is the tether line density, A_{sol} (0.89) is the tether annulus solidity, L_{ref} (32 000 m) is the total tether length in the deployer, E (1.4) is the area exponent, f_θ (0.18) is the friction coefficient over the exit guide, θ_0 (0) is the zero friction exit angle, f_n is the friction coefficient over the brake pole, and n^* is the number of effective brake turns of the tether on the barberpole.

4 Numerical results

4.1 YES2 phase 1 deployment optimization

The mission parameters at the time of writing this paper are specified as a combination of the orbital parameters and tether properties. The deployment is to be separated into two phases. The first phase requires

that 3.5 km of tether be deployed as close to the local vertical as possible. The second phase requires the tether to be deployed to 30 km with the correct swing velocity. However, only the first phase is considered here. The perigee altitude is 249 km, and the apogee altitude is 285 km. Thus, the orbit semimajor axis is 6645 km and the eccentricity is 0.0027 (subject to variations in Earth radius). The true anomaly at the time of the initial ejection is assumed to be very close to 0 degrees. The orbit inclination is 63.03 deg, argument of perigee is 62.249 deg, and the right ascension of the ascending node is 124.142 deg. The ejection is to take place at 3:15UTC on the 20th of September 2007. The initial separation between the payload and the mother satellite is taken to be 3.0 m, and the ejection velocity is 2.58 m/s. The other system properties are approximate and are taken to be: payload mass $m_{\text{sub}} = 12$ kg, payload drag product $C_D A_{\text{sub}} = 0.4$ m^2, mother satellite mass 6530 kg, mother satellite drag product $C_D A_m = 10.0$ m^2, tether diameter $d = 0.5$ mm, exospheric temperature $T_{\text{ex}} = 1000$ K.

The trajectory of the system is optimized using the rigid tether model and the flexible tether model. Details of the rigid tether optimization may be found in [17]. The cost function selected for minimization is the length acceleration

$$\mathcal{J} = \int_{\tau_0}^{\tau_f} (\Lambda'')^2 \, \mathrm{d}\tau. \tag{87}$$

The boundary conditions for the deployment in the rigid model are set precisely using terminal constraints

$$[\theta, \theta', \phi, \phi', \Lambda, \Lambda']_{t=t_f} = [0, 0, \text{free}, \text{free}, 1, 0]. \tag{88}$$

No constraints are imposed on the out-of-plane angles because of the effects of aerodynamic drag, which continually force changes in the out-of-plane dynamics over an orbit.

The flexible tether is optimized using a polynomial expansion with $n = 11$ and four internal nodes. The tether is discretized into 10 elements for the optimization, but the results shown here are given for 40 tether elements. Because the length variation is already one that minimizes the length acceleration, the cost function for minimization is

$$J = \left[\sin\theta_{\text{sub}}(\nu_f)\right]^2 + \left[\theta_1'(\nu_f)\right]^2 + 5\left[\theta_{\text{sub}}'(\nu_f)\right]^2 + 10\sum_{j=1}^{n}\left\{\left[\theta_j''(\nu_f)\right]^2 + \left[\phi_j''(\nu_f)\right]^2\right\} \tag{89}$$

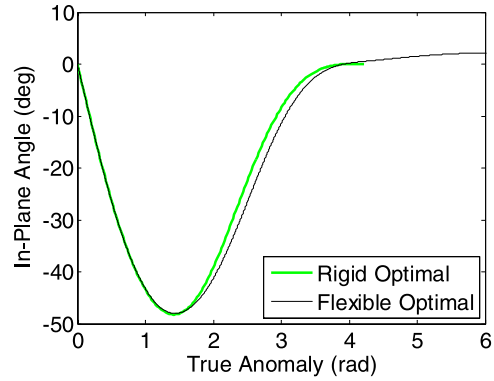

Fig. 3 YES2 deployment optimization showing in-plane tether angle

which is selected to drive the system to an quasi-equilibrium position near the local vertical.

The rigid tether model was optimized with the time domain discretized into 240 segments. The flexible tether model equations of motion are propagated using a variable-order, variable-step integrator implemented in C++. The flexible tether system was initially optimized using adaptive simulated annealing [28], and the solution was later refined using SNOPT. A typical optimization takes between 10 and 30 minutes, depending on the initial guess used.

Results for the deployment optimizations are shown in Figs. 3 through 9. Figure 3 shows the in-plane libration angle versus the orbit true anomaly expressed in radians. The deployment time is allowed to be a free variable and only the results of the optimization for the rigid tether are shown, whereas the simulation of the flexible tether deployment continues after deployment has completed. The results show good agreement between the two deployment schemes, particularly during the first half of the deployment. The rigid tether is deployed slightly more quickly than the flexible tether. The effects of aerodynamic drag are apparent in the flexible tether after the tether has been deployed (deployment finishes at approximately 4.3 rad), where the in-plane angle is driven to approximately 2 degrees. This angle remains almost constant with time beyond the results shown in Fig. 3. Figure 4 shows the tether length during the deployment, which illustrates how close the two sets of results are. It is evident that both deployment schemes are very smooth. Figure 5 shows the deployment rate, which illustrates the key differences in the two deployment profiles. The flexible tether is slowed down faster at the be-

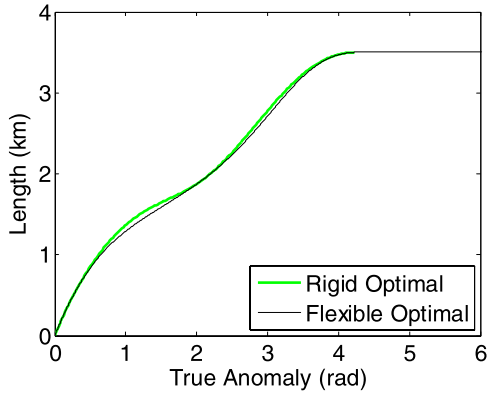

Fig. 4 YES2 deployment optimization showing tether length

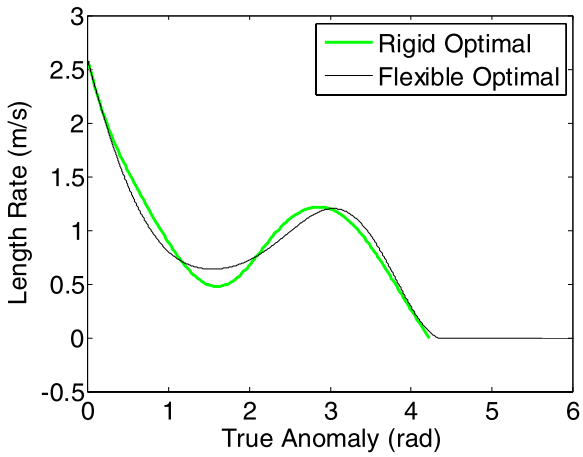

Fig. 5 YES2 deployment optimization showing deployment speed

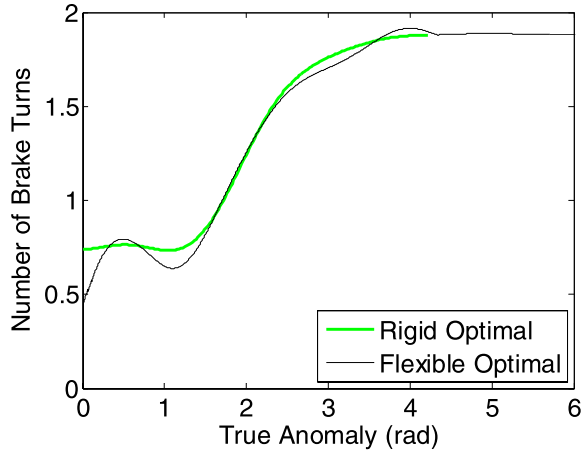

Fig. 6 YES2 deployment optimization showing number of turns on friction pole

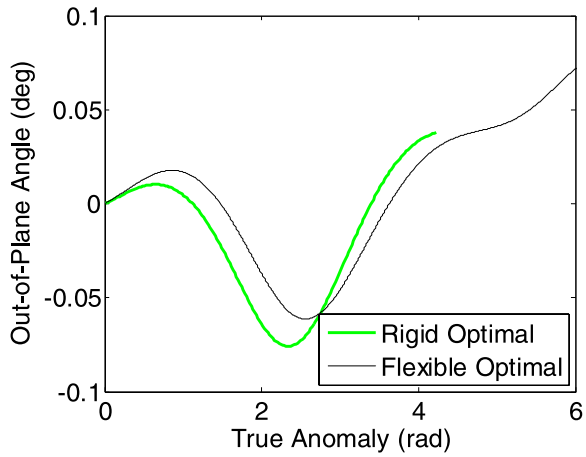

Fig. 7 YES2 deployment optimization showing out-of-plane angle

ginning of the deployment, but the minimum in the length rate seen at approximately 1.5 rad is larger than the 0.5 m/s observed for the rigid tether. The average faster deployment during this time is actually desirable due to concerns that uncertainties in the deployment hardware could cause the tether to stop deploying prematurely. A higher deployment speed provides more tolerance for these uncertainties. Figure 6 shows the number of brake turns on the friction pole required to achieve the optimal deployment. It is at this level that the differences in the deployment profiles become most pronounced. The number of brake turns for the rigid tether is almost constant at 0.74 initially, whereas the flexible tether starts at approximately 0.44, increases to approximately 0.8, then decreases to 0.64, before finally increasing to the steady-state value of about 1.9. Figure 7 shows the out-of-plane angle of the tether, which is less than 0.1 deg over the entire deployment. The differences in the two trajectories can be attributed to the slightly different drag calculations and variation in the tether shape in the flexible tether case. The absolute difference between the two is very small, however. Figure 8 shows projections of the tether shape during the deployment, shown every 0.1 rad. The tether remains quite straight during the deployment process, which shows that the lateral tether oscillations are kept to a minimum. Note that this is not true for arbitrarily chosen deployment profiles, particularly in the presence of aerodynamic drag. The convergence of the tether to the quasi-steady-state equilibrium position can be seen at the end of the de-

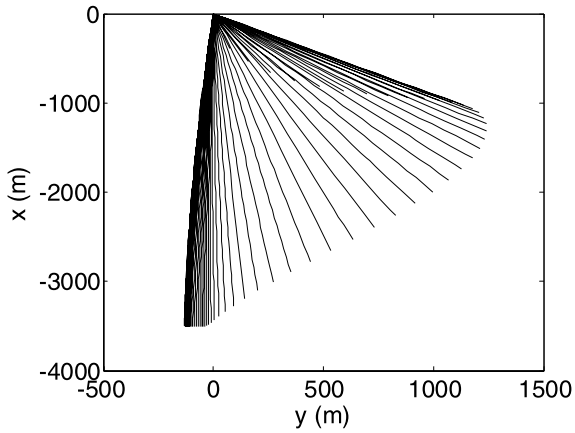

Fig. 8 YES2 deployment optimization showing flexible tether shape at intervals of 0.1 rad

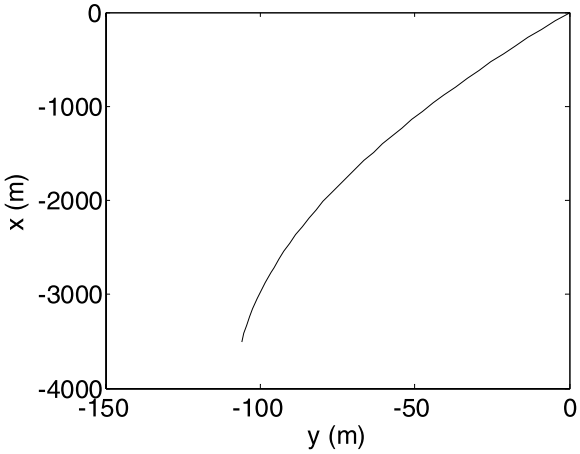

Fig. 9 YES2 deployment optimization showing quasi-steady in-plane tether shape after 7 rad

ployment. Figure 9 shows the shape of the tether at a true anomaly of 7 rad, illustrating the fact that the tether is curved due to the higher drag near the subsatellite compared to the drag near the mother satellite. These results clearly illustrate the power of the method for optimization of flexible tether trajectories, where the use of only 4 optimization parameters is able to generate results consistent with an optimization of a rigid tether carried out with 240 parameters used in the control discretization.

4.2 Tethered satellite retrieval

As a final example, the method developed in this paper is applied to the more difficult problem of retrieval of a subsatellite with a flexible tether. Retrieval is generally more difficult than deployment because disturbances tend to be amplified. The case of a rigid tether is much simpler, since the effects of tether flexibility are not considered. The retrieval parameters are selected to be: orbit eccentricity, $e = 0.01$, semimajor axis $a = 7000$ km, subsatellite mass $m_{\text{sub}} = 200$ kg, and tether density $\rho = 0.0005$ kg/m. All other orbital and system properties are the same as in the YES2 deployment example. The cost for the rigid tether optimization is selected as one of minimum length acceleration. The boundary conditions are for the tether to commence fully deployed at the local vertical, and for the tether to be retrieved to 10% of its original length in 6 rad (approximately one orbit). The problem is discretized using 100 time segments in the case of a rigid tether. Optimization with the flexible tether is performed with the tether length approximated with polynomials up to degree $n = 14$. The number of internal optimization parameters is selected to be 6. The tether is discretized into 10 elements for the optimization, but numerical simulation results are shown for 40 elements. In the flexible tether optimization, the initial and final tether length accelerations are constrained to be zero, whereas for the rigid tether they are allowed to be free. The cost function to be minimized is selected as

$$J = 100\{[\sin\theta_{\text{sub}}(\nu_f)]^2 + [\theta_1'(\nu_f)]^2\} + 5[\theta_{\text{sub}}'(\nu_f)]^2 + 10\sum_{j=1}^{n}\{[\theta_j''(\nu_f)]^2 + [\phi_j''(\nu_f)]^2\}. \quad (90)$$

Numerical results are shown in Figs. 10 through 14. Figure 10 shows the variation in the in-plane libration angle during the retrieval for both a rigid tether and a flexible tether. In this case, because the retrieval time is fixed, there appears to be much better agreement between the two sets of optimal results. Figure 10 shows nearly identical agreement in the variation of the tether libration angle during the retrieval. It is evident that the retrieval is very smooth, with the angle not exceeding approximately 35 degrees. Figure 11 shows the variation in tether length for the retrieval, showing near exact agreement between the two methods. The retrieval is conducted without any need to reverse the direction of the tether reel. Again, the smooth behavior of the retrieval is easily seen. Figure 12 shows the retrieval rate of the tether, which peaks at approximately -0.9 m/s. This low maximum retrieval rate is due to the short

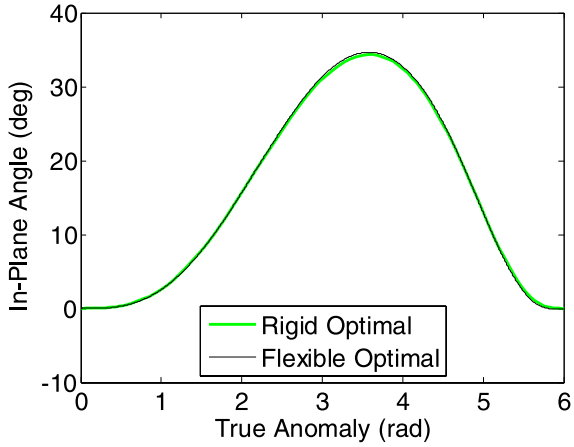

Fig. 10 Retrieval optimization showing in-plane tether angle

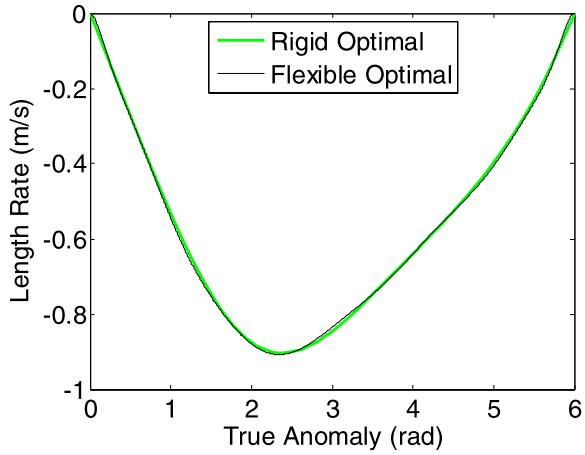

Fig. 12 Retrieval optimization showing tether length rate

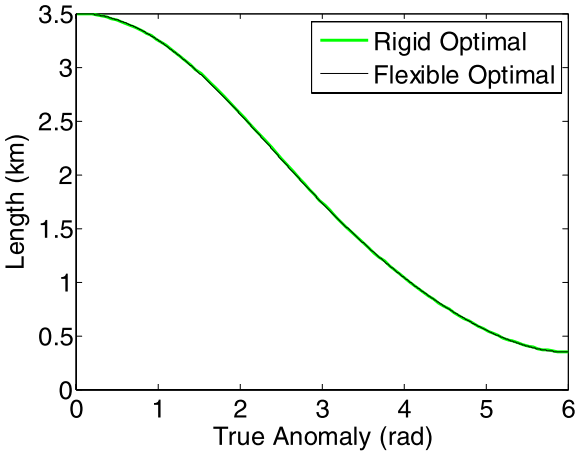

Fig. 11 Retrieval optimization showing tether length

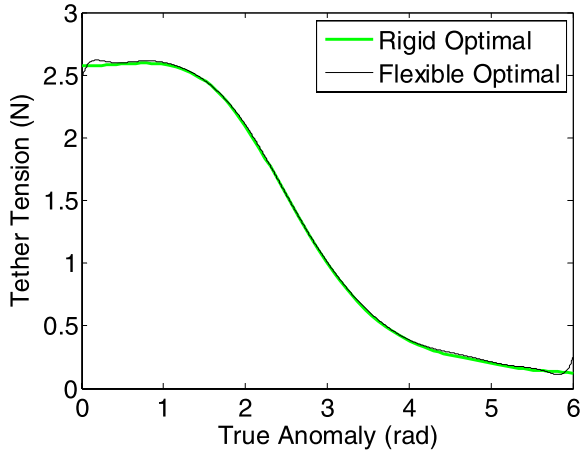

Fig. 13 Retrieval optimization showing tether tension

tether length (3.5 km). However, the smooth behavior of the retrieval makes this scheme particularly desirable. Note that Fig. 12 illustrates some small differences in the retrieval rate at the beginning and ends of the process. This is due to the effects of constraining the length acceleration at the boundaries. This becomes most evident in the tether tension history, as shown in Fig. 13. The general shape and magnitude of the tension history is in excellent agreement between the rigid and flexible models except at the boundaries. Initially, the tension is lower at the initial time in the flexible tether case because the length acceleration is zero. For the rigid tether, the length acceleration is negative at the initial time, requiring a higher level of tension. The reverse is true at the final time. The implication is that the tension would need to "jump" slightly after the completion of the retrieval if the rigid tension profile is used. However, these effects are dynamic, and do not influence the resulting trajectories to any significant degree. Finally, Fig. 14 shows projections of the flexible tether shape during the retrieval at time intervals of 0.1 rad. It can be seen that any lateral vibrations are suppressed by using the proposed optimization methodology.

The results for tether retrieval make it clear that modeling only the libration dynamics is sufficient as a first step in control design. In general, the author has found that the accuracy of controllers developed using low-order approximations depends the way the tether is controlled. For example, if the tether length varies smoothly, then excellent agreement is obtained between an inflexible and flexible tether model. How-

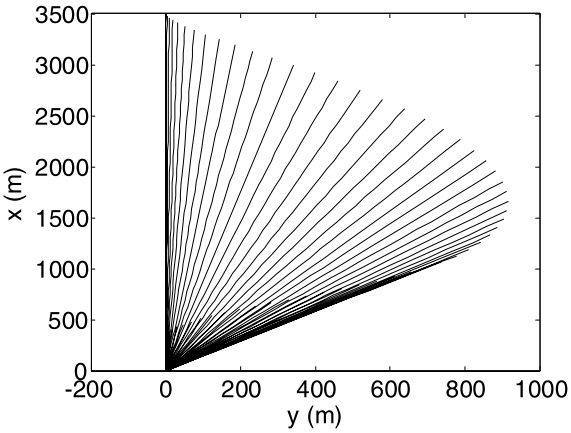

Fig. 14 Retrieval optimization showing flexible tether shape every 0.1 rad

ever, when the tether length changes suddenly, or the tension becomes very low, then significant lateral oscillations can be induced, which can cause large errors in the models. In [5], it was shown that the use of optimal control to minimize the variation in tether length acceleration or tension rate is desirable. The use of an inflexible tether model is always recommended as a first step because of the relative simplicity. However, for more detailed design for a particular mission, the use of flexible tether model is essential to ensure that the tether is well-behaved during deployment, and that the tether librations will meet the desired requirements.

5 Conclusions

A methodology for optimizing the deployment and retrieval of tethered satellites has been presented. For the case of a tether modeled as an inelastic rod, direct transcription methods can be applied. However, the resulting trajectories neglect lateral tether vibrations, which can be important during the retrieval phase. An efficient multibody model that treats the tether as inelastic, but flexible, was derived to enable optimizations to be carried out. The control problem is converted into a parameter optimization problem through a discretization of the tether length history in terms of Chebyshev polynomials. Minimum length acceleration over the trajectory is specified a priori, together with boundary conditions for the tether length and length rate. The shape of the deployment profile is then optimized by specifying the values of the tether length at a few points during the deployment. The deployment/retrieval profiles are implemented via tension control using commanded values of the length, length rate, and length acceleration. Numerical results show that very few optimization parameters are required to successfully deploy or retrieve a flexible tether with high accuracy.

Acknowledgements Portions of this research were undertaken while a Research Fellow at RMIT University, Melbourne, Australia under the supervision of Prof. Pavel Trivailo. I would like to thank Andrew Hyslop and Marco Stelzer for helpful discussions about the YES2 deployment problem.

References

1. Misra, A.K., Modi, V.J.: A survey on the dynamics and control of tethered satellite systems. Adv. Astronaut. Sci. **62**, 667–719 (1987)
2. Fujii, H.A., Anazawa, S.: Deployment/retrieval control of tethered subsatellite through an optimal path. J. Guid. Control Dyn. **17**, 1292–1298 (1994)
3. Barkow, B., Steindl, A., Troger, H., Wiedermann, G.: Various methods of controlling the deployment of a tethered satellite. J. Vib. Control **9**, 187–208 (2003)
4. Lakso, J., Coverstone, V.L.: Optimal tether deployment/retrieval trajectories using direct collocation. In: AIAA/AAS Astrodynamics Specialist Conference, 14–17 August 2000. AIAA Paper 2000-4349 (2000)
5. Williams, P., Trivailo, P.: On the optimal deployment and retrieval of tethered satellites. In: 41st AIAA/ASME/SAE/ASEE Joint Propulsion Conference, Tucson, AZ, July 2005. AIAA Paper 2005-4291 (2005)
6. Lorenzini, E.C., Bortolami, S.B., Rupp, C.C., Angrilli, F.: Control and flight performance of tethered satellite small expendable deployment system-II. J. Guid. Control Dyn. **19**, 1148–1156 (1996)
7. Carroll, J.A.: SEDS deployer design and flight performance. In: AIAA Space Programs and Technologies Conference and Exhibit, Huntsville, AL, September 1993. AIAA Paper 93-4764 (1993)
8. Williams, P., Blanksby, C., Trivailo, P., Fujii, H.A.: Receding horizon control of tether system using quasilinearisation and Chebyshev pseudospectral approximations. In: AAS/AIAA Astrodynamics Specialists Conference, Big Sky, MT, 3–7 August 2003. Paper AAS 03-535 (2003)
9. Williams, P., Blanksby, C., Trivailo, P.: Optimisation of tether assisted sample return from the international space station. In: Australian International Aerospace Congress, Brisbane, Australia, 29 July–1 August 2003. Paper AIAC 2003-021 (2003)
10. Misra, A.K., Modi, V.J.: Deployment and retrieval of shuttle supported tethered satellites. J. Guid. Control Dyn. **5**, 278–285 (1982)
11. Fujii, H., Ishijima, S.: Mission function control for deployment and retrieval of a subsatellite. J. Guid. Control Dyn. **12**, 243–247 (1989)

12. Fujii, H., Uchiyama, K., Kokubun, K.: Mission function control of tethered subsatellite deployment/retrieval: in-plane and out-of-plane motion. J. Guid. Control Dyn. **14**, 471–473 (1991)
13. Vadali, S.R., Kim, E.S.: Feedback control of tethered satellites using Lyapunov stability theory. J. Guid. Control Dyn. **14**, 729–735 (1991)
14. Bainum, P.M., Kumar, V.K.: Optimal control of the shuttle-tethered-subsatellite system. Acta Astronaut. **7**, 1333–1348 (1980)
15. Koakutsu, H., Nakajima, A., Ota, S., Nakasuka, S.: Tension control of micro tether system on circular orbit considering tether flexibility. J. Space Technol. Sci. **12**, 1–13 (1996)
16. Zimmerman, F., Schottle, U.M., Messerschmid, E.: Optimal deployment and return trajectories for a tether-assisted re-entry mission. In: AIAA Atmospheric Flight Mechanics Conference, Portland, OR, August 1999. AIAA Paper 99-4168 (1999)
17. Williams, P., Hyslop, A., Stelzer, M., Kruijff, M.: YES2 optimal trajectories in presence of eccentricity and aerodynamic drag. In: International Astronautical Congress, Valencia, Spain, October 2006
18. Crellin, E.B., Janssens, F., Poelaert, D., Steiner, W., Troger, H.: On balance and variational formulations of the equations of motion of a body deploying along a cable. J. Appl. Mech. **64**, 369–374 (1997)
19. Wiedermann, G., Schagerl, M., Steindl, A., Troger, H.: Simulation of deployment and retrieval processes in a tethered satellite system mission. In: International Astronautical Congress, Amsterdam, The Netherlands, October 1999
20. Xu, D.M., Misra, A.K., Modi, V.J.: Thruster-augmented active control of a tethered subsatellite system during its retrieval. J. Guid. Control Dyn. **9**, 663–672 (1986)
21. Kim, E., Vadali, S.R.: Modeling issues related to retrieval of flexible tethered satellite systems. J. Guid. Control Dyn. **18**, 1169–1176 (1995)
22. Ross, I.M.: A roadmap for optimal control: the right way to commute. Ann. New York Acad. Sci. **1065**, 210–231 (2005)
23. Elnagar, G., Kazemi, M.A., Razzaghi, M.: The pseudospectral Legendre method for discretizing optimal control problems. IEEE Trans. Autom. Control **40**, 1793–1796 (1995)
24. Ross, I.M., Fahroo, F.: Legendre pseudospectral approximations of optimal control problems. Lect. Notes Control Inf. Sci. **295**, 327–342 (2003)
25. Williams, P.: User's guide to DIRECT version 1.17. Technical Report, Melbourne, Australia, April 2005
26. Gill, P.E., Murray, W., Saunders, M.A.: SNOPT: an SQP algorithm for large-scale constrained optimization. SIAM J. Optim. **12**, 979–1006 (2002)
27. Betts, J.T.: Practical Methods for Optimal Control Using Nonlinear Programming. Advances in Control and Design Series. SIAM, Philadelphia (2001)
28. Ingber, A.L.: Adaptive simulated annealing (ASA): lessons learned. Control Cybern. **25**, 33–54 (1996)